

AMERICAN UNIVERSITY OF BEIRUT

THESIS RELEASE FORM

ENHANCEMENT OF THE STABILITY AND THE
PHOTOLUMINESCENCE QUANTUM YIELD OF CESIUM
LEAD HALIDE PEROVSKITES BY LIGAND DOPING

I warrant that the American University of Beirut is the copyright owner or exclusive licensee of the thesis, that the work meets all the requirements for the submission of the thesis, and that I have obtained the necessary permission for the reproduction of the work in any form.

I am of the age of majority

I have signed this form in the presence of my thesis advisor

by
CHRISTINA EDWARD AL TAWIL

I have read and understand the contents of this form

A thesis
submitted in partial fulfillment of the requirements
for the degree of Master of Science
to the Department of Chemistry
of the Faculty of Arts and Sciences
at the American University of Beirut

Beirut, Lebanon
April 2022

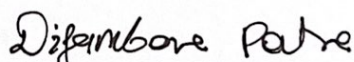
AMERICAN UNIVERSITY OF BEIRUT

ENHANCEMENT OF THE STABILITY AND THE
PHOTOLUMINESCENCE QUANTUM YIELD OF CESIUM
LEAD HALIDE PEROVSKITES BY LIGAND DOPING

by

CHRISTINA EDWARD AL TAWIL

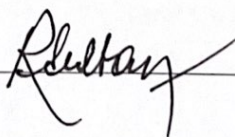
Approved by:



Signature

Dr. Digambara Patra, Professor
Department of Chemistry

Advisor



Signature

Dr. Rabih Sultan, Professor
Department of Chemistry

Member of Committee



Signature

Dr. Tarek Ghaddar, Professor
Department of Chemistry

Member of Committee

Date of thesis defense: April 28, 2022

THESIS RELEASE FORM

Student Name: Al Tawil Christina Edward
Last First Middle

I authorize the American University of Beirut, to: (a) reproduce hard or electronic copies of my thesis; (b) include such copies in the archives and digital repositories of the University; and (c) make freely available such copies to third parties for research or educational purposes:

- As of the date of submission
- One year from the date of submission of my thesis.
- Two years from the date of submission of my thesis.
- Three years from the date of submission of my thesis.

Signature



Date 5/5/2022

ACKNOWLEDGEMENTS

First and foremost, praises and thanks to the God, the Almighty, for His showers of blessings throughout my research work to complete the research successfully.

I would like to express my deepest appreciation to my advisor and mentor Professor. Digambara Patra for his patience and support throughout my master's journey. I thank him for giving me this opportunity to conduct research in his lab and under his invaluable guidance. He assisted me develop my research project, enriched my scientific knowledge, and supported me to continue and never give up. Without his guidance and patience this work would not have been possible.

I would like to acknowledge my committee members, Professor. Rabih Sultan, and Professor. Tarek Ghaddar for the knowledge and experience they shared with me during my graduate courses. Moreover, I would like to thank them for the useful comments and advice they provided me to get the best out of this work.

I owe a deep sense of gratitude to Dr. Tony Khoury from the Department of Chemistry at the Lebanese University for his continuous encouragement and support leading me toward the chemistry field. I thank him for his confidence in my abilities.

My sincere thanks go to the best research assistant, Misses Riham El Kurdi Maksoud, who was constantly by my side supporting and giving me infinite encouragement. I thank her for all the experience and useful tips she gave me which helped me ace my research project. I would like to thank her for her dual friendship and assistantship roles throughout my journey.

Heartful thanks to my best lab mates; Justine, Hanine and Saaedeh for always believing in me and motivating me. I'm extremely blessed for the really unique friendships I made on this journey. To all my graduate colleagues: Fatat, Cynthia, Daniela, Amira, Amar, Mariam, and Mohamad thank you for being a part of my journey.

A special thanks goes to Kamal A. Shair Central Research Laboratory's (KAS, CRSL) members; Ms. Rania Chatila, Mr. Chady Assaf and Dr. Juan Younes for their technical support and valuable assistance.

Finally, I would like to dedicate this work to my loving parents, my father Edward and my mother Rania, whose words of encouragement and push for tenacity ring in my ears. No words can express my endless gratitude and sincere appreciation for your constant motivation and wholehearted support throughout all stages of my life. Without your endless genuine caring, support, motivation, and prayers for me, I don't know where I would be today. I hope I met all your trust and faith in me. I am who I am because of you, thank you.

ABSTRACT

OF THE THESIS OF

Christina Edward Al Tawil

for

Master of Science

Major: Chemistry

Title: Enhancement of the Stability and Photoluminescence Quantum Yield of Cesium Lead Halide Perovskites by Ligand Doping

In general, perovskites are nanoparticles having a crystalline structure. These nanoparticles attracted scientists' attention due to their great potential in various fields ranging from chemical and industrial fields to biomedical fields. Unfortunately, cesium lead halide perovskites suffer from their high instability, where they undergo a rapid chemical decomposition within time. For this purpose, three different reaction parameters were varied starting from the time of the reaction, going to the concentration of lead bromide, and ending by the concentration of cesium oleate. Moreover, surfactant ligands were used to control the synthesis of inorganic perovskite nanoparticles. In our work, the synthesis of cesium lead halide perovskites was carried out based on the hot injection method. Henceforth, the prepared perovskites have been characterized using UV-Visible absorption spectroscopy, fluorescence spectroscopy, scanning electron microscopy, thermogravimetric analysis, and X-Ray diffraction technique.

On the first hand, it was found that the most stable CsPbBr₃ perovskites were formed when mixing 0.15 g (C=0.06812 M) of lead bromide heated for 40 minutes, with a volume of 1.2 mL of cesium oleate (C=0.0092 M). Henceforward, either hexadecyltrimethylammonium Bromide (CTAB) or hexadecylpyridinium Bromide (CPB) were used as an ecofriendly surfactant to increase in the first place; the stability of the formed perovskites, and later on to boost their photoluminescence quantum yield (PLQY). Hence, the addition of CTAB had proven its efficiency on the formed CsPbBr₃ nanoparticles by increasing their thermal stability and by enhancing their PLQY till 75%. Henceforth, the addition of CPB showed remarkable effects by increasing thermal stability, boosting the PLQY to 90%, preserving the crystal structure of CsPbBr₃, and preventing the anion exchange between Br⁻ and I⁻ upon the addition of low concentrations of PbI₂.

On the second hand, CsPbI₃ perovskites undergo rapid chemical decomposition and transformation into yellow δ -phase. Thus, it is imperative to develop a stabilized black phase for photovoltaic applications. For this purpose, a surfactant ligand was used to control the synthesis of inorganic perovskite CsPbI₃ nanoparticles. Herein we demonstrate a new avenue for lead halide perovskites with the addition of either CTAB or silica nanoparticles (SiO₂ NPs) to maintain in the first place; the stability of the α -CsPbI₃ phase, and later to boost their photoluminescence quantum yield (PLQY).

Keywords: inorganic perovskites, optimization, lead halide, α -CsPbI₃, CsPbBr₃, CTAB, CPB, silica nanoparticles, PLQY, anion exchange.

TABLE OF CONTENTS

ACKNOWLEDGEMENTS	1
ABSTRACT	2
ILLUSTRATIONS	8
TABLES	10
ABBREVIATIONS	11
INTRODUCTION	12
A. Definition	12
B. Structure.....	13
C. Classification	15
1. Inorganic Oxide Perovskites.....	15
2. Halide Perovskites	16
D. Properties	17
1. Dielectric properties.....	17
2. Optical properties.....	18
3. Photoluminescence quantum yield	18
4. Ferroelectricity.....	19
5. Superconductivity	19
6. Piezoelectricity.....	20
7. Multiferroicity.....	20
8. Colossal Magneto Resistance (CMR).....	21
9. Catalytic activity	21
E. Methods of synthesis	22

1.	Solid-state reactions	22
2.	Gas phase preparation	23
3.	Wet chemical (solution) methods	23
4.	Co-precipitation method	24
5.	Hydrothermal synthesis	24
6.	Sol-gel method	25
7.	Microwave synthesis.....	25
8.	Combustion method.....	26
F.	Applications of perovskites	27
1.	Sensors and biosensors	27
2.	Catalysts.....	28
3.	Solar cells.....	30
4.	Solar-oxide fuel cells	30
5.	Optoelectronic applications	31
6.	Other applications	31
G.	Limitations and solutions.....	32
1.	Degradation.....	32
2.	Stability.....	32
3.	Material toxicity.....	32
H.	Aims.....	33
MATERIALS AND METHODS		35
A.	Materials	35
B.	Sample preparation	35
C.	Instrumentation	36
D.	Optimization of the reaction parameters.....	38
E.	Stabilization of the synthesized perovskites	38
F.	Photoluminescence enhancement of the perovskites.....	38

CHARACTERIZATION AND OPTIMIZATION OF THE REACTION PARAMETERS IN THE SYNTHESIS OF CESIUM LEAD BROMIDE PEROVSKITES40

A. Introduction..... 40

B. Methods of preparation 41

 1. Effect of reaction time 41

 2. Effect of cesium oleate concentration..... 41

 3. Effect of lead bromide concentration..... 42

C. Results and discussion 42

 1. Optimization of the reaction parameters..... 43

 2. Crystallinity analysis of lead bromide perovskites 53

D. Conclusion 55

ENHANCEMENT OF THE STABILITY AND PHOTOLUMINESCENCE QUANTUM YIELD OF CESIUM LEAD BROMIDE PEROVSKITES BY HEXADECYLTRIMETHYLAMMONIUM BROMIDE DOPING56

A. Introduction..... 56

B. Methods of synthesis 57

 1. Preparation of CTAB solution 57

 2. Effect of CTAB..... 57

C. Results and discussion 58

 1. Photoluminescence stability of CsPbBr₃ in the presence/absence of CTAB.. 58

 2. Thermal stability of CsPbBr₃ in the presence and absence of CTAB..... 61

 3. Photoluminescence quantum yield in the presence/absence of CTAB..... 62

D. Conclusion 65

HEXADECYLPYRIDINIUM BROMIDE AS A NEW CAPPING AGENT FOR THE CRYSTAL STRUCTURE PRESERVATION OF CESIUM LEAD BROMIDE PEROVSKITES.....66

A. Introduction.....	66
B. Methods of preparation.....	67
1. Preparation of CPB solution.....	67
2. Effect of CPB/ CTAB.....	67
3. Effect of PbI_2	67
C. Results and discussion.....	68
1. Characterization of CsPbBr_3 perovskites prepared in the presence of CPB and CTAB.....	68
2. Thermal stability of CsPbBr_3 in the presence of either CPB or CTAB.....	70
3. Photoluminescence quantum yield in the presence of CPB and CTAB.....	72
4. Variation in the photoluminescence of CsPbBr_3 upon the addition of PbI_2 in the presence of either CPB or CTAB.....	73
D. Conclusion.....	75

CESIUM LEAD IODIDE PEROVSKITES IN THE PRESENCE OF CTAB LIGAND FOR HIGHER TIME STABILITY AND BETTER PHOTOLUMINESCENCE QUANTUM YIELD76

A. Introduction.....	76
B. Methods of preparation.....	77
1. Effect of CTAB-oleate solution.....	77
2. Effect of SiO_2 -oleate solution.....	78
C. Results and discussion.....	79
1. Synthesis of lead iodide perovskites.....	79
2. Time-dependent stability CsPbI_3 in the presence of CTAB.....	88
3. PLQY measurements in the presence/absence of CTAB and SiO_2 NPs.....	91

D. Conclusion	92
CONCLUSION	93
REFERENCES	95

ILLUSTRATIONS

Scheme

Scheme 1 Schematic representation of a typical 3D structure of ABC_3 perovskites.....	12
Scheme 2 Schematic representation of the unit cell of ABC_3 perovskite	13

Figure

1. Classification of perovskites.	15
2. Schematic representation of the $CsPbX_3$ synthesis.	36
3. (A) UV-Visible spectra and (B) fluorescence emission spectra of lead bromide perovskites having different reaction times.	44
4. SEM images of lead bromide perovskites at (A) 0 min; (B) 10 min(C) 20 min; and (D) at 40 min.	46
5. Color change of $CsPbBr_3$ solution with the increase of Cs-oleate concentration	47
6. (A) UV-Visible spectra; and (B) fluorescence emission spectra of lead bromide perovskites after adding different masses of cesium oleate.	48
7. SEM images of lead bromide perovskites with different masses of cesium oleate (A) 7.53 mg; (B) 15.07 mg; and (C) 22.60 mg.	50
8. Color change of $CsPbBr_3$ solution with the increase of lead bromide concentration	51
9. (A) UV-Visible spectra and (B) fluorescence emission spectra of lead bromide perovskites using different masses of lead bromide.....	52
10. SEM images of lead bromide perovskites having different masses of lead bromide (A) 0.08 g; (B) 0.15 g; and (C) 0.2 g.	53
11. X-Ray Diffractogram pattern of $CsPbBr_3$ prepared using the optimized method and lead bromide precursor.	54
12. Fluorescence emission intensity of $CsPbBr_3$ (A) in the absence of CTAB; (B) in the presence of CTAB; and (C) the plot of I/I_0 for $CsPbBr_3$ in the absence and presence of CTAB within time from 0 to 60 hours.....	59
13. The difference in the shape of PL intensity peaks in the absence and the presence of CTAB after 60 hours.....	60
14. Thermogravimetric analysis TGA of lead bromide perovskites.	61

15. PLQY (%) of CsPbBr ₃ in the absence of CTAB at 40°C and 200°C	63
16. PLQY variation in the presence and the absence of CTAB.....	64
17. (A) UV-Visible spectra and (B) fluorescence emission spectra of lead bromide perovskites prepared using different capping agents.	69
18. SEM images of lead bromide perovskites with the addition of either (A) CPB or (B) CTAB.....	70
19. Thermogravimetric analysis TGA of lead bromide perovskites.	71
20. PLQY variation in the presence and the absence of either CPB or CTAB.....	72
21. Variation of the fluorescence emission intensity of CsPbBr ₃ upon the addition of PbI ₂ (A) in the presence of CTAB and (B) in the presence of CPB.	74
22. Cesium lead iodide perovskites solution (A) before centrifugation; and (B) after centrifugation.	79
23. Color solution of cesium lead halide perovskites in the absence and presence of CTAB (A) before centrifugation; and (B) after centrifugation.	80
24. X-Ray Diffractogram pattern of CsPbI ₃ prepared in the absence and presence of CTAB	81
25. (A) Fluorescence emission spectra of CsPbI ₃ prepared in the absence or presence of CTAB; (B) UV-Visible spectra of CsPbI ₃ prepared in the absence and presence of CTAB.	83
26. SEM image of CsPbI ₃ prepared in the presence of CTAB.	84
27. TGA analysis of CsPbI ₃ prepared in the presence of CTAB; cesium carbonate; lead iodide; and CTAB.....	85
28. X-Ray diffractogram pattern of CsPbI ₃ prepared in the presence of SiO ₂ NPs	86
29. (A) UV-Visible spectra of CsPbI ₃ prepared in the presence of SiO ₂ NPs; (B) Fluorescence emission spectra of CsPbI ₃ prepared in the presence of SiO ₂ NPs	87
30. (A) SEM image of CsPbI ₃ prepared in the presence of SiO ₂ NPs; and (B) TGA analysis of CsPbI ₃ prepared in the presence of SiO ₂ NPs.	88
31. Solution color of CsPbI ₃ after 4 consecutive days in the presence of CTAB (left side) and in the presence of SiO ₂ NPs (right side).	89
32. (A) Variation of the fluorescence emission intensity of α-CsPbI ₃ in the presence of CTAB within time; (B) Maximum emission intensity vs time for α-CsPbI ₃ solution in the presence of CTAB	90
33. Color change of α-CsPbI ₃ in the presence of CTAB solution within time.	91

TABLES

Table

1. Emission wavelength of PbBr_2 and CsPbBr_3 at different time.	45
2. PLQY % of CsPbBr_3 at different time and temperature.	63
3. Different PLQY values obtained in the literature	65
4. Different PLQY values obtained in the literature.	73
5. Different PLQY (%) values found in the literature for CsPbI_3 perovskites.....	92

ABBREVIATIONS

Br⁻: Bromide ion
Cs-oleate: Cesium oleate
Γ: Iodide ion
OA: Oleic acid
OAm: Oleylamine
ODE: 1-Octadecene
CPB: Hexadecylpyridinium bromide
CTAB: Hexadecyltrimethyl-ammonium bromide
PbX₂: lead halide
PLQY: Photoluminescence quantum yield
SEM: Scanning electron microscopy.
SiO₂ NPs: Silica nanoparticles.
TGA: Thermogravimetric analysis.
UV-Vis: Ultraviolet-visible spectrometry.
XRD: X-Ray Diffractogram.

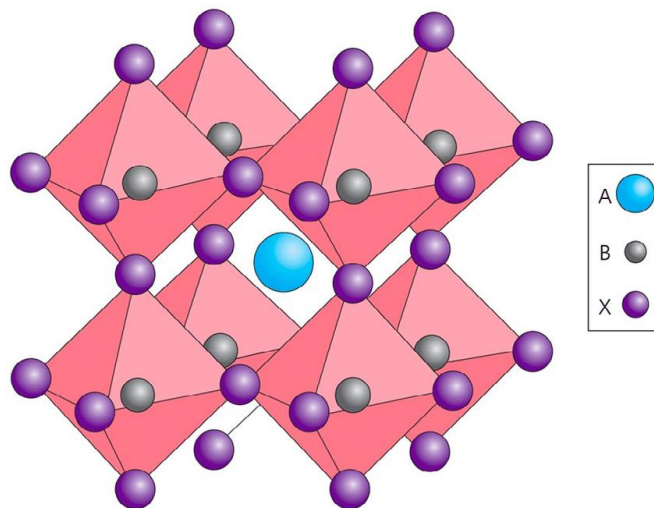
CHAPTER I

INTRODUCTION

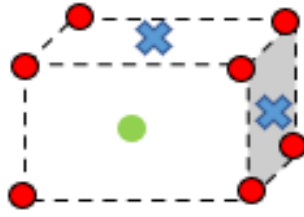
A. Definition

Perovskite was discovered by the Geologist Gustav Rose in the Ural Mountains of Russia in 1839. It was named in honor of the Russian mineralogist Lev Perovski. It is a naturally occurring mineral made of calcium titanium oxide and have a CaTiO_3 as its chemical formula and having a yellow, brown or black color [1].

Perovskites are compounds that have a general chemical formula of ABC_3 and having a cubic or tetragonal crystal structure, where A and B are metal cations and C is an anion (scheme 1). An octahedron of C ions surrounds the B ions present on the corners of a three-dimensional cube and the A cation is embedded in the center of the cube to neutralize the charge of the structure. Thus, the ratio is 1:1:3 [2]. According to scheme 2; A is the center of cube (ratio 1), B on the corners of the cube ($8 \times (1/8) = 1$), and C in the face-centered of the cube ($6 \times (1/2) = 3$).



Scheme 1 Schematic representation of a typical 3D structure of ABC_3 perovskites [3].



Scheme 2 Schematic representation of the unit cell of ABC_3 perovskite

The perovskite structure has been illustrated to be the most versatile ceramic host [4]. Depending on what atom it is formed from, perovskites show distinct variety of properties such as dielectric properties [5], optical properties [6], ferroelectricity [7], superconductivity [8], piezoelectricity [9], multiferroicity [10] and catalytic activity [11].

This diversity of properties made the perovskites useful for various applications such as gas sensor [12], glucose sensor [13], neurotransmitters sensor [14], catalyst [15] and solar cells [16].

Indeed, several synthesis methods were developed and improved to synthesize pure Perovskites. For instance, solid-state reaction [17], gas phase preparation [18], wet chemical methods (solution methods) [19], co-precipitation methods [20], hydrothermal synthesis [21], sol-gel method [22], CVD process and microwave synthesis [23] are widely used in the production process.

Moreover, controlling the composition of the solution and phase transition engineering leads to the optimization of the material [24].

B. Structure

The ideal form of perovskite oxides is ABO_3 having the cubic structure. In its cubic unit cell, atom A ion has the largest radius; 12-fold coordinated by oxygen anions

and is located on the corners of the cube at corner position (0, 0, 0). Oxygen atoms are at the face center of the cubic lattice at position (½, ½, 0). Tetravalent B cations lie within oxygen octahedral and occupy the body center position (½, ½, ½) in a 6-fold coordination [25].

However, at different temperatures, phase transitions occur, and the crystal structure varies. For low temperatures, below 100 K, perovskites obtain a stable orthorhombic (γ) phase. As temperature increases, this phase will be replaced by a tetragonal (\square) phase; and at very high temperatures above 330 K, a stable cubic (α) phase replaces the tetragonal phase [26].

Moreover, substitution of A/B sites results in deviation from the ideal form and the formula becomes $A_{1-x}A'B_{1-y}B'O_3$. This cubic distortion results in orthorhombic, rhombohedral, hexagonal, or tetragonal structure. Tolerance factor "t" is used to calculate the real measure of the degree of distortion.

$$t = \frac{r_A + r_O}{\sqrt{2}(r_B + r_O)} \quad [27] \quad (\text{where } r \text{ is the radii of the ions})$$

Perovskites occur in 3 types of structures; the first type contains localized electrons, the second type contains delocalized energy-band states and the third type is a transition between the two types [28]. It has a very flexible composition which enables it to incorporate different ions of various sizes and charges. Thus, it exists in different forms such as double perovskite, layered perovskite, triple perovskite etc. [29].

Perovskite formation has 3 requirements [30]:

- The constancy of the octahedron which is represented by the octahedron factor m.
- The electro-neutrality of the charges where the sum of charges of cations and anions is neutral.

- The ionic radii requirements ($r_A > 0.090$ nm and $r_B > 0.051$ nm and $0.8 < t < 1$).
- Otherwise, the structure will be distorted, and this affects its physical properties.

C. Classification

Perovskites crystal structure is versatile, and it is able to accommodate a diverse range of cations with different oxidation states. Thus, a classification based on the composition of the perovskite AMX_3 crystal structure has been attempted by several researchers. In fact, perovskites are classified into two categories: inorganic oxide perovskites and halide perovskites (See Figure 1).

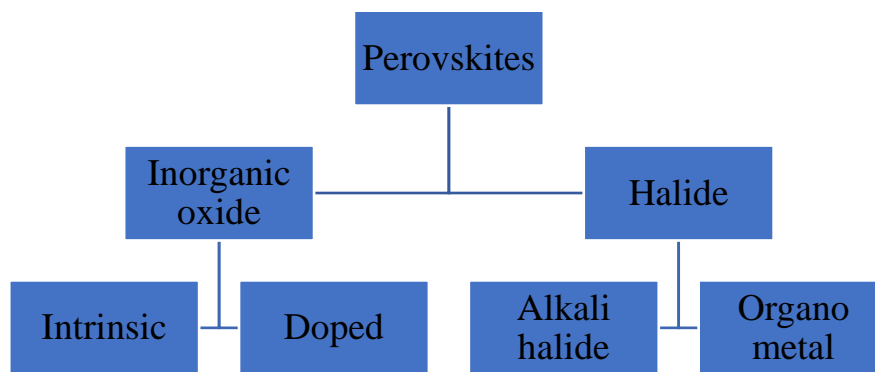


Figure 1 Classification of perovskites.

1. *Inorganic Oxide Perovskites*

These perovskites have a general structure of AMO_3 or A_2MO_4 . First, in AMO_3 structure, A-site cation is 12-fold coordinated and M-site cation is 6-fold coordinated with oxygen anions. However, in A_2MO_4 structure, AMX_3 layers are alternated with AO layers.

Oxide perovskites have various physical properties such as ferroelectricity, catalytic activity, ferromagnetism, piezoelectricity, superconductivity, and high

electrical conductivity [31]. They are further classified into **intrinsic** perovskites and **doped** perovskites.

a. Intrinsic perovskites

These perovskites have a higher power conversion efficiency compared to other perovskites. This ensures their very high stability and long lifetime.

b. Doped perovskites

These perovskites have different properties, compared with un-doped, since the crystal structure is changed. For example, doping the perovskite with lead or a halide leads to an increase in stability and efficiency [32].

2. *Halide Perovskites*

This type has an AMX_3 structure and is divided into alkali-halide perovskites and organo-metal perovskites.

a. Alkali-halide perovskites

In this type, perovskites are composed of monovalent alkali metal A, a divalent metal M, and a halogen anion X. Example, $KPbI_3$ used for solar cells. This type has low energy loss and wider bandgap which increases power conversion efficiency [33].

b. Organo-metal perovskites

Herein, the perovskite is composed of an organic cation A (can be aliphatic or aromatic), a divalent metal cation M, and a halogen anion X. This type has a large absorption coefficient and a tunable bandgap. It is used in optoelectronic devices such

as solar cells, field effect transistors (FETs), electronic devices and photovoltaic applications [34].

D. Properties

Perovskites exhibit various properties due to their chemical structure. For instance, the non-stoichiometry of the anions and/or cations, the mixed valence, partial substitution of ions and the distortion of the configuration affects the perovskites properties.

Perovskites substitution leads to various properties such as ferroelectricity (BaTiO_3), superconductivity (BaYCu_3O_7), piezoelectricity ($\text{Pb}(\text{Zr,Ti})\text{O}_3$), electrical conductivity (LaCrO_3), ion conductivity (CaTiO_3), magnetism (LaFeO_3), and catalytic activity (LaCoO_3) [35].

1. Dielectric properties

A dielectric material is a poor conductor of electricity upon applying a direct current voltage. But it supports electrostatic field and stores energy, thus it can be inserted into capacitors to improve its function [36].

Ferroelectricity is one of the inherent properties to dielectric materials, and it is related to its crystal structure. These properties are essential for electro-ceramics; thus, several methods were used to prove the dielectric properties in a material. One of these methods was Relaxor ferroelectric. Using this method, BaTiO_3 was subjected to three phase transitions. The crystal structure changes as temperature increases, however at high temperatures above 303 K, it returns to cubic structure and no ferroelectric behavior is observed due to the slow reduction processes at high temperature.

Therefore, BaTiO₃ perovskite showed high dielectric constant and generated high dipole moment [37].

2. *Optical properties*

Perovskites have excellent optical and photoluminescence properties.

On the first place, tunable emission; upon controlling the stoichiometry or substitution of halides, inorganic-perovskite such as CsPbX₃ can act as a light emitter in the visible range [38]. Hence, inserting organic molecules or replacing some ions could also lead to tuning the emission near IR or UV regions [39].

On the second place, perovskites are well known to have high quantum yield efficiency which measures the percentage of converted photons into radiation relative to the number of absorbed photons. Perovskite has a high quantum efficiency due to the presence of the bandgap with almost no charge-trapping states [40].

Furthermore, quantum confinement effect depends on the size of the semiconductor where it should be smaller than Bohr radius. Therefore, changing the size of radii affects the optical absorption and emission properties [41].

3. *Photoluminescence quantum yield*

The photoluminescence quantum yield (PLQY) is one of the most essential photophysical properties of perovskites for optoelectronic and solar cell applications.

PLQY of a material is defined as the number of photons emitted as a fraction of the number of photons absorbed. Thus, PLQY is a key performance indicator of the efficiency of the synthesized material.

$$= \frac{\int F(\lambda_{em})}{\int F_R(\lambda_{em})} \frac{A_R(\lambda_{ex}) n^2}{A(\lambda_{ex}) n_R^2} \quad (\text{Equation 1})$$

PLQY is determined based on Equation 2 and it always takes values between 0 and 1 [42]. Where η is the PLQY, $\int F(\lambda_{em})$ is the integrated intensity of emission, $A(\lambda_{ex})$ is the percentage of light absorbed at the excitation wavelength, n is the refractive index, and the subscript R denotes the reference data.

4. Ferroelectricity

Ferroelectricity leads to a spontaneous electric polarization of the material when subjected to an external electric field [7]. Ferroelectric materials are known for having a high dielectric constant with magnitude twice higher than normal dielectric materials.

For instance, barium titanate (BaTiO_3) unit cells are aligned; however, no polarization is observed without external field. In the presence of external field, BaTiO_3 becomes a ferroelectric material and generates high dipole moment [37]. Perovskites show high and unique ferroelectricity reaction, and this property is useful in several purposes such as: capacitors, IR cameras, vibration sensors, and imaging devices [4].

5. Superconductivity

Superconductivity is the phenomenon whereby under certain conditions; the material allows the passage of electricity and expels its magnetic field. In fact, there are 2 groups of superconducting oxide perovskites. The first group is Cu-based perovskites such as La-Ba-Cu-O, where Cu can act as a high temperature superconductor. The superconductivity is related to the Cu-O layers present in the structure [43]. The second group is metal oxide perovskites, these compounds have a ratio of 2:3 (2 metal atoms to every 3 oxygen atoms) [44]. This group has a higher transition temperature than Cu-based perovskites and contains a mixture of alloys and metallic compounds.

In fact, perovskites electronic conductivity can be enhanced by doping A site with other cations, leading to an increase in the number of mobile charge carriers [37].

6. Piezoelectricity

This property is defined as the capacity of a material to produce electrical charge upon being applied to a mechanical stress [10]. The polarization degree is proportional to the applied mechanical strain [9]. Piezoelectric materials require external force, however, in ferroelectric materials there is a spontaneous interaction between its dipoles. Thus, all ferroelectrics are piezoelectric, but not all piezoelectric are ferroelectric.

Perovskites showing piezoelectricity make it useful in several applications such as: sensors, cigarette lighters, microphones, modulators, nano-positioning in AFM and STM, etc. [45]

7. Multiferroicity

Perovskites materials have the capability to use their both magnetization and polarization states simultaneously [46]. Multiferroic perovskites have crystalline structure and are composed of transition metal oxides including rare-earth manganite and ferrites [47].

In fact, to have ferromagnetic and ferroelectric ordering, the material should be made of insulator metals [48]. Ferroelectricity is produced upon distorting the highly symmetrical structure of the material. This distortion allows electric polarization of the material. Magnetic spin ordering can produce ferroelectricity as well in absence of structural distortion [49].

8. *Colossal Magneto Resistance (CMR)*

CMR is known as an extreme change in the electrical resistance of the material due to the presence of magnetic field. It mainly affects manganese-based perovskite oxides. For instance, divalent alkaline-earth ion doped perovskites $RE_{1-x}AE_xMnO_3$, where RE is trivalent rare-earth (La, Pr, Sm, etc.) and AE represents divalent alkaline-earth ions (Ca, Sr, Ba), exhibit CMR effect which makes them have a great potential application in spintronic. In fact, the orbital occupancy and orbital order of manganese ions affects the magnetic phase [50].

9. *Catalytic activity*

Perovskites are chemically stable which makes it exhibit various catalytic activities such as: automobile exhaust gas catalyst, intelligent automobile catalyst and cleaning catalyst. It can be described as a model of active sites and acts as oxygen activated catalyst for materials with oxygen deficiency. Interestingly, perovskites containing Cu, Co, Mn, or Fe showed a great catalytic action toward degrading NO at high temperatures. In fact, degrading NO is a very difficult catalytic reaction ($2NO \rightarrow N_2 + O_2$). However, due to oxygen deficiency and eliminating oxygen in the products, perovskites showed an excellent catalytic activity. Doping the perovskite or performing the experiment in oxygen rich atmosphere will enhance perovskites' ability to degrade NO [51].

Another catalyst replaces some of the precious metals with fine particles and have a high surface to volume ratio. However, this catalyst is being deactivated due to the non-stable fine particles. Thus, perovskite oxides are used since they show redox properties to preserve scattering state. Upon reduction, fine metal bids of Pb are

produced having radius of 1-3 nm. This leads to partial replacement and sedimentation of Pb in the structure of the perovskite upon exposing the catalyst to redox atmosphere. This leads to the removal of the pollutant Pb from exhaust gas. The excellent stability of the perovskite and the great dispersion state of Pb lead to naming the catalyst as an intelligent catalyst [37].

E. Methods of synthesis

All the previously discussed physical and chemical properties are affected by the synthesis of a perovskite. Several synthesis methods were developed and improved to overcome the drawbacks and synthesize a pure compound. For example: solid-state reactions, gas phase preparation, wet chemical methods, co-precipitation methods, hydrothermal synthesis, sol gel method, etc.

1. Solid-state reactions

Using this method, both raw materials and products are in the solid state. First, the ions are mixed in a specific ratio to obtain a product with the desired composition. These ions are ball milled in acetone or isopropanol and then dried at 100°C and calcined in air 600°C for 4-8 hours. The obtained product is ground, sieved and recalcined to obtain the final product with the desired composition. For example, synthesis of $\text{BaCe}_{0.95}\text{Yb}_{0.05}\text{O}_{3-\delta}$ was done by mixing BaCO_3 , CeO_2 and Yb_2O_3 [17].

Usually, perovskite oxides ceramics are synthesized using this method at high temperature. However, this technique has several disadvantages such as: presence of impurities during grinding and heating, presence of defects which will affect luminescence, and coarseness of particles which affect their coating ability [52].

2. Gas phase preparation

Gas phase preparation is used to form perovskite films with specific thickness and composition. Several techniques such as: Laser ablation [53], molecular beam epitaxy [54], DC sputtering [55], magnetron sputtering [56], electron beam evaporation and thermal evaporation [57] were developed for gas phase deposition [18].

It is categorized into 3 types depending on the deposition. First type is depositing at the crystallization temperature under suitable atmosphere. Second type is depositing at low temperature followed by post-annealing at high temperature. And the third type is depositing at intermediate temperature followed by post-annealing treatment [18]. For example, Yttrium barium copper oxide ($\text{YBa}_2\text{Cu}_3\text{O}_7$) films are synthesized by co-evaporating Y, Cu and BaF_2 then annealing them at high temperature in a suitable atmosphere containing O_2 wet with water vapor to reduce the hardening time and substrate interaction [58].

3. Wet chemical (solution) methods

It is used to synthesize a double-perovskite compound which is homogeneous and has a large surface area. It includes sol-gel preparation, co-precipitation of metal ions and thermal treatment. Wet method has several advantages: it requires lower temperature than solid-state reactions, improved reactivity, greater flexibility in forming thin films, better homogeneity, low cost, and better control of particle size, stoichiometry, and purity.

In fact, there are two methods for the separation of solvent from perovskite. First method includes the precipitation of the perovskites followed by the filtration process which separate solid from liquid. The second method comprises the

thermal treatment which removes the solvent by evaporation, sublimation, combustion etc. Moreover, solubility, solvent compatibility, cost, purity etc. play an important role in choosing the suitable method [23].

4. Co-precipitation method

Synthesis of simple oxides occurs by precipitating metal salts using a reagent to decrease solubility. Co-precipitation is a simultaneous precipitation of several metal salts using different cations and under certain temperature, pH, and concentration to obtain a homogenous product. The co-precipitation occurs when using chemical reagents to decrease solubility such as: urea, ammonia, ammonium carbonate or ammonium oxalate. The formed oxide could result from: oxalate-based precipitation, as well as acetate, citrate, hydroxide, or cyanide-based precipitations. For example, in acetate-based precipitation, different acetate ions are mixed with metal ion salts and then calcined in air to synthesize $\text{La}_{1-x}\text{Sr}_x\text{CoCO}_3$ perovskite [20].

5. Hydrothermal synthesis

The reaction is performed in an aqueous solution and under a high temperature and pressure conditions to produce crystalline powder without the need of calcination [21]. By controlling the reaction temperature, pH, time and reactant concentration; the size and shape of the perovskite can be optimized. Also, the temperature of the reaction could be decreased by using electric field. For example, synthesizing BaTiO_3 could be performed at lower temperature using electric field [59].

There are two methods to thermally treat a reaction, either by freeze-drying or plasma spray-drying. Freeze drying occurs by dissolving the salt in a suitable solvent to

become homogenous and directly freezing the solution. Then the frozen solution will be freeze-dried to get the dehydrated salt which will be grinded into perovskite powder [23]. On the other hand, plasma spray-drying occurs by injecting the reactants and interacting with molten droplets. By varying the plasma parameters, temperature and post-decomposition parameters, a superconducting oxide is synthesized.

6. *Sol-gel method*

Sol-gel alkoxide method was the first method used to synthesize non-silicate ceramics perovskites [22]. This method was used in hydrolysis and polycondensation of metallic alkoxides which leads to the synthesis of oxide compounds [60].

Sol-gel method was used to prepare nanosized particles and complex cation phases. However, the chemical composition of complex oxides is difficult to be controlled and the precursor is unstable. Thus, in aqueous medium, the precursors used are inorganic agents and chelating agents of carboxylic acid or polyols. On the other hand, one of the main advantages of this method is that it can synthesize thin films at low temperatures [61].

7. *Microwave synthesis*

Microwave irradiation process (MIP) is a method used to synthesize perovskites nanomaterials using lower temperature and reduced time [23]. Perovskites use microwave irradiation as a heat source to be synthesized. It has several advantages such as: fast rate of reaction, finer particles, higher surface area, efficient and clean energy.

There are two methods of microwave synthesis: the microwave-assisted hydrothermal method and the solid-state microwave.

Initially, microwave-assisted hydrothermal synthesis which combines the microwave and hydrothermal methods, demands the polarizing of a material through irradiating it with microwave radiation under high temperature and pressure conditions.

Secondly, the solid-state microwave, which is specific for simple compounds such as oxides, while for complex compounds, such as chalcogenides, the synthesis should be combined with other methods such as: combustion, sol-gel or hydrothermal methods [62]. Many perovskites were prepared using MIP since it synthesizes crystalline particles in shorter time, higher surface area and finer particles. In addition, Pb-containing perovskites can be synthesized using MIP because it is a simple and fast method, so it minimizes the loss of Pb [63].

8. Combustion method

This method is based on a redox reaction between a fuel and an oxidant leading to the production of a homogeneous perovskite powder with large surface area. This method saves time and uses less energy while producing ultra-fine powder.

Citrate/nitrate combustion is an example of solution combustion where metal ions are the oxidant and citric acid is the fuel. Nitrates act as auto-catalyst that remain in the solution and facilitates auto-combustion process, instead of eliminating them in the form of NO_x .

Many nano-phasic thin films were prepared using this process due to its several advantages such as: high purity, ability to control the composition of the perovskite, and homogeneity. Two steps are required; a complex is formed between the citric acid and the metal ions, then the formed complex is poly-esterified with ethylene glycol, this leads to a homogeneous solution of the metal salts in the gel [23].

F. Applications of perovskites

Perovskites have a wide range of application depending on its chemical and physical properties. Inorganic perovskite oxides exhibited great properties such as: electronic conductivity, thermal and chemical stability, ions mobility in the crystal structure, super-magnetic property, photocatalytic activity, etc. These properties allowed perovskites to have wide applications in catalysis, fuel cells, electrochemical sensing, capacitors etc.

1. Sensors and biosensors

a. Gas sensors

The material used as a gas sensor should be hydrothermally stable, resistant to poisoning, adapts present technologies, has suitable electronic structure and good similarity with target gases [64]. Several perovskite oxides are used for different gas sensing due to their thermal stability, ideal band gap, and the difference between cations of A and B sites which allow the doping of the perovskite [12].

b. Glucose sensors

It is necessary to detect H_2O_2 which is an oxidizing agent and glucose which is a fundamental metabolite of many living organisms. Glucose and H_2O_2 play an important role in clinic, pharmaceutical analyses, chemical and food industries [13].

There are two types of sensors: enzymatic and non-enzymatic sensors. However, enzymatic sensors are not stable and are affected by pH, temperature, poisoning substances, humidity etc. Inorganic perovskite oxides can act as a non-enzymatic

glucose sensor since they exhibit various properties for glucose sensing such as: ferroelectricity, high thermostability, catalytic activity, etc. [65].

c. Neuro-transmitters sensors

Dopamine (DA) is a neurotransmitter that plays an important role in the brain and body, its deficiency leads to Parkinson's disease. However, ascorbic acid (AA) and uric acid (UA) interfere with DA so the detection of dopamine will be hard unless the presence of a modified surface which is sensitive and selective.

For example, modifying carbon paste electrode with SrPdO₃ (CpE/SrPdO₃) allows it to detect dopamine in the presence of AA and UA [66]. This enhanced the selectivity, sensitivity and anti-interfering ability. It also enhanced the catalytic activity which is due to the interaction of the oxygen atoms of the hydroxyl group and the transition element of the perovskite. Thus, an oxygen-surface interaction takes place between oxygen atoms and the surface of perovskite which is deficient of oxygen [14].

2. *Catalysts*

Several perovskites showed catalytic activity in hydrogen evolution reactions (HER), oxygen evolution reactions (OER) and reduction reactions due to its surface, solid-state and morphological properties [37].

a. Hydrogen evolution reactions (HER)

HER has several advantages such as: cleaner energy, plentiful sources, and high heat of combustion. This reaction could be used in metal-electrode position, acid corrosion, energy production and hydrogen oxidation reaction. Several characteristics

are required for the raw materials of this reaction: high stability, large active surface area and essential electro-catalytic activity. The activation energy, reaction order and rate determining step are important factor when choosing the suitable perovskite [2].

b. Oxygen reduction and oxygen evolution reactions

Oxygen reduction reactions (ORR) and oxygen evolution reactions (OER) have various applications such as: fuel cells, water electrolysis, cathodic protection, etc. There are many catalysts for ORR and OER reactions such as platinum-based catalyst and precious metal oxides. However, they are expensive and rare. So, the best ones are those of low cost like metal oxide perovskites of transition and rare earth metals.

Perovskite oxides act as an electro-catalyst for these reactions. For example, $\text{La}_{0.6}\text{Ca}_{0.4}\text{CoO}_3$ shows a high catalytic activity in basic medium, high conductivity and large surface area [67].

3. Solar cells

Solar cells are considered as a green source of energy which is cleaner than fossil fuels. Silicon based photovoltaic solar cells transform the solar energy into electrical energy, but silicon is expensive so a substitute of low cost should be used.

Solar cells based on organic/inorganic solid-state ammonium lead halide ($\text{CH}_3\text{NH}_3\text{PbX}_3$) have high conversion efficiency, low cost and its raw materials are available. Thus, it is a better substitute for silicon based solar cells. These materials have the essential properties needed for photovoltaic applications: high conversion efficiency, high stability, suitable band gap, low temperature etc. [68].

Though MAPbX_3 perovskites have great potential in solar cell applications, the major serious pitfalls of these materials are that they degrade rapidly when exposed to ambient conditions with moderate humidity [69]. These limitations have induced the increased study of new compositions such as the all-inorganic cesium lead halide (CsPbX_3) perovskites.

4. Solar-oxide fuel cells

Fuel cells are a cleaner source of energy, which uses chemical fuel as an energy source and convert it into electrical energy. Fuel cells have several advantages such as: energy efficient, low emissions, zero noise pollution, distributed nature and its ability to be used in future hydrogen fuel economy. Solid oxide fuel cell (SOFC) is one of the most common types of fuel cells.

Perovskites can be utilized as anode or cathode for SOFC and show high catalytic performance depending on the fuel type and temperature. For example,

$\text{Ba}_{0.5}\text{Sr}_{0.5}\text{Co}_{0.8}\text{Fe}_{0.2}\text{O}_3$ can act as a cathode for SOFC under a temperature of 500°C and using a humidified H_2 as fuel [70].

5. *Optoelectronic applications*

a. Optical lasing

Metal halide perovskites has a high absorption coefficient, strong photoluminescence, and amplified spontaneous emission. When a material is put in optical cavity, lasing occurs. Here, perovskites' crystal is a naturally formed cavity, so it can achieve lasing without the need of optical cavity. For example, lasing is observed in $\text{CH}_3\text{NH}_3\text{PbX}_3$. Moreover, changing the composition of perovskite can control the emission wavelength and the lasing spectrum [71].

b. Light emitting diodes (LED)

Metal halide perovskites can be used in light emitting diodes because of several advantages such as: low cost, high performance, easy preparation, high color purity, and color tenability over a wide spectrum by changing the content of halides in the compound.

Quantum dots perovskites are preferred in LEDs since their small size limits exciton diffusion and thus increases radiative recombination. Interestingly, inorganic perovskites such as CsPbX_3 are used in LED applications [72].

6. *Other applications*

Perovskites are also used in FETs, photodetectors, single photon emitters, capacitors, storage and switching devices etc. For example, perovskite nanoplates were

used to fabricate FET [73] and $\text{CH}_3\text{NH}_3\text{PbI}_3$ nanowires were used to fabricate photodetectors [74].

G. Limitations and solutions

There are some challenges that limited the commercialization of perovskites especially the perovskite solar cell (PSC). Main challenges include degradation, lack of stability and material toxicity.

1. Degradation

Humidity is one of the factors leading to degradation of perovskite. The interaction between water molecules and perovskite materials leads to instability of these materials [75]. A possible solution would be isolating it from external environment by encapsulating the material [76], or by using hot injection method of synthesis.

2. Stability

Operational stability of the material is affected by light, heat, and oxygen. These factors are involved in reactions which degrade the material [77]. A suitable solution would be using stabilizing agents such as Cesium and Rubidium [78].

3. Material toxicity

The main concern is the hazardous exposure to lead. The use of lead in perovskites affects the environment as well as its degradation. However, the quantity used in perovskites is nothing compared to the use of lead in batteries.

Lead perovskites has a high-power efficiency. A possible solution would be the use of lead alternative such as tin perovskites; however, they have lower power conversion efficiency. To solve this problem, lead poisoning was studied by testing the effect of rain with different water pH's. It was concluded that the use of lead in perovskite is environmentally safe [78].

H. Aims

After presenting the information related to perovskites, we will focus in our work on the synthesis of stable cesium lead halide perovskites with high photoluminescence quantum yield. For this purpose, our work will be divided into 2 essential parts:

Chapter II includes the materials used, the method of perovskites preparation, in addition to the application that will be developed.

Chapter III will emphasize the mechanism of the synthesis of CsPbBr_3 in addition to the optimization of the reaction parameters, to obtain the most stable and smallest in size perovskite nanoparticles. The reaction parameters that are optimized are as follows: the effect of reaction time, concentration of cesium oleate and concentration of lead halide.

Moreover, in chapter IV, hexadecyltrimethylammonium Bromide (CTAB) is used as an ecofriendly surfactant to increase in the first place; the physical/thermal stability of the formed perovskites, and later on to boost their photoluminescence quantum yield (PLQY).

In Chapter V, hexadecylpyridinium Bromide (CPB) is used as a new capping agent for the crystal structure preservation of cesium lead bromide perovskites. The effect of lead iodide doping on the photoluminescence emission will be studied as well.

Finally, Chapter VI will include the synthesis of cesium lead iodide CsPbI_3 based on the hot-injection method and using the optimization results obtained in chapter III. Furthermore, either hexadecyltrimethylammonium Bromide (CTAB) or silica nanoparticles will be used as a capping agent to stabilize in the first place; the α - CsPbI_3 phase, and to increase the photoluminescence intensity and boost their quantum yield.

CHAPTER II

MATERIALS AND METHODS

A. Materials

Cesium Carbonate (Cs_2CO_3), 1-Octadecene (ODE, $\text{C}_{18}\text{H}_{36}$), Oleylamine (OAm, $\text{C}_{18}\text{H}_{37}\text{N}$), Lead (II) iodide (PbI_2), Rohdamine 6G ($\text{C}_{28}\text{H}_{31}\text{N}_2\text{O}_3\text{Cl}$), Hexadecyltrimethylammonium bromide (CTAB, $\text{C}_{19}\text{H}_{42}\text{BrN}$), Hexadecylpyridinium bromide (CPB, $\text{C}_{21}\text{H}_{38}\text{BrN}$), and Sulphuric acid (H_2SO_4) were all obtained from Acros Organics. Lead (II) bromide (PbBr_2) was acquired from Fisher Scientific Company. Colloidal silica (SiO_2), Oleic acid (OA, $\text{C}_{18}\text{H}_{34}\text{O}_2$) and hexane (C_6H_{14}) were purchased from Sigma Aldrich. Quinine anhydrous ($\text{C}_{20}\text{H}_{24}\text{N}_2\text{O}_2$) was acquired from Fluka Analytical. Ethanol ($\text{C}_2\text{H}_6\text{O}$) was purchased from Honeywell Riedel-de Haen. All chemicals were used as received without further purification.

B. Sample preparation

To start with, Cs-oleate was prepared by mixing 0.4 g of Cs_2CO_3 ($C = 0.053 \text{ M}$) with 20 mL ODE and 1.24 mL OA into a vial. The solution was stirred and heated at 200°C until complete dissolution of cesium carbonate. After complete dissolution, the solution color turned from transparent to yellow verifying the formation of cesium oleate. Cs-oleate solution was sealed and stored at room temperature for further use.

The preparation of cesium halide perovskites was carried out using hot injection method (see Figure 2).

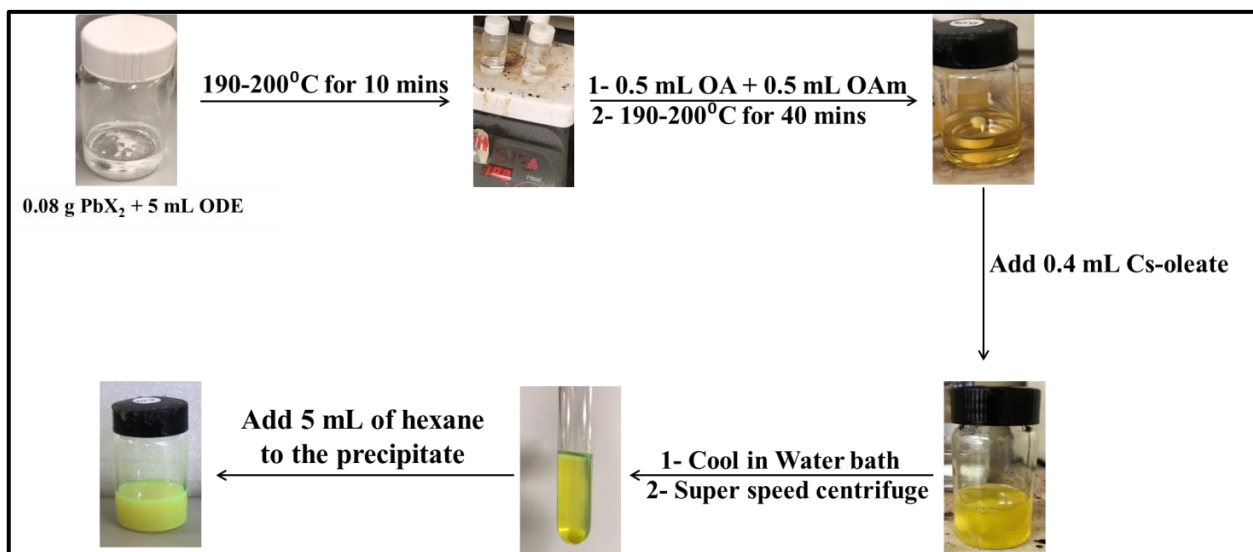


Figure 2 Schematic representation of the CsPbX₃ synthesis.

In the first place, 0.08 g of lead halide was mixed with 5 mL ODE in an air free environment at 190-200 °C for 10 min. Then 0.5 mL OA and 0.5 mL OAm were added, and the mixture was left until complete dissolution of PbX₂ in solution. Next, 0.4 mL of Cs-oleate was added to the solution and immediately immersed in a cold-water bath (T= 10⁰C), in order to ensure the formation of the perovskites. Finally, the solution was centrifuged at 15000 rpm for 15 minutes and the precipitate was dissolved in 5 mL hexane and used for further characterization.

C. Instrumentation

Initially, the optical properties of the formed perovskites were studied using ultraviolet-visible (UV-vis) spectroscopy. JASCO V-570 UV-VIS-NIR spectrophotometer was used to record the absorption spectra at room temperature in a wavelength range of 200-800 nm in a 3 mL cuvette.

Fluorescence emission spectra were measured using a Jobin-Yvon-Horiba Fluorolog III fluorometer and the FluorEssence program. The excitation source was a

100 W Xenon lamp, and the detector used was an R-928 operating at a voltage of 950 V instrument. The excitation and emission slits width were kept at 5 nm. Briefly, 0.2 mL from the initial solution were pipetted and diluted with hexane into a total volume of 3 mL.

The X-ray diffraction (XRD) data were used to examine the structural properties of the perovskites. These data were recorded using a Bruker d8 discover X-ray diffractometer equipped with Cu-K α radiation ($\lambda=1.5405^\circ$). The monochromator used was Johansson type. The X-ray scans were done for 2θ between 5° and 55° . The step size was 0.02 s and the scan rate was 20 s per step. For the X-Ray study, few drops of the CsPbX₃ were deposited on the zero-background holder and the analysis was conducted.

Thermogravimetric Analysis (TGA) measurements were done using a Netzsch TGA 209 in the temperature range 30 to 900°C with an increment of 15 °C/ minute in a N₂ atmosphere. For this purpose, a few μ L were measured in the Al₂O₃ crucible, and then placed in the oven at 45°C to evaporate the hexane. The complete evaporation of hexane was verified by the consistency of the crucible mass after 20 minutes.

Scanning Electron Microscopy (SEM) was used to determine the surface morphologies of the perovskite structure. This analysis was done using Tescan, Vega 3 LMU with Oxford EDX detector (Inca XmaW20). In short, lead perovskite solution was deposited on an aluminum stub and coated with carbon conductive adhesive tape.

D. Optimization of the reaction parameters

Physical properties such as the size and shape depend intensely on the reaction parameters. For this reason, the reaction parameters were optimized in order to prepare the most stable lead halide perovskites. The parameters that were modified are:

- Effect of reaction time
- Concentration of PbX_2
- Concentration of Cs-oleate

The synthesized perovskites were characterized using spectroscopic and microscopic techniques to choose the optimum conditions.

E. Stabilization of the synthesized perovskites

Unfortunately, cesium lead halide perovskites suffer from their high instability, where they undergo a rapid chemical decomposition within time. For this purpose, an ecofriendly surfactant was needed to enhance the physical/thermal stability of the solution. Two stabilizing agents were tested:

- Effect of CTAB
- Effect of SiO_2 NPs
- Effect of CPB

F. Photoluminescence enhancement of the perovskites

After optimizing the reaction parameters and choosing the suitable surfactant, cesium lead halide perovskites were proved to show:

- Increasing photoluminescence intensity
- Boosting photoluminescence quantum yield

- Variation of photoluminescence emission due to PbI_2

It is necessary to mention that the sample preparation for each part is developed in the specific chapter.

CHAPTER III

CHARACTERIZATION AND OPTIMIZATION OF THE REACTION PARAMETERS IN THE SYNTHESIS OF CESIUM LEAD BROMIDE PEROVSKITES

A. Introduction

The morphology of a perovskite is one of the most critical factors that influence the efficiency of the material. For this reason, it is critical to optimize the synthesis conditions.

Indeed, several synthesis methods were developed and improved to produce pure perovskites. For instance, solid-state reactions [17], gas phase preparation [18], wet chemical methods (solution methods) [79], co-precipitation methods [20], hydrothermal synthesis [21], sol-gel method [22], chemical vapor deposition (CVD) process and microwave synthesis [23] are widely used in the production process.

Lead halide perovskites nanowires could be synthesized using CVD process. This process is based on vapor-liquid-solid mechanism, where metal films are used as a catalyst to enhance the 1D crystal growth. One limitation of this method is the low growth temperature of the perovskite. Another synthesis method is solution method without using surfactant ligand.

Moreover, despite the synthesis method adopted, controlling the process parameters such as concentration of precursors, reaction time, and addition of solvents, play an essential role in the perovskites' quality, crystallinity, crystal size, conversion of precursor to perovskite and efficiency. The formation of the perovskite depends strongly on the precursor's concentration, temperature, environment, etc. [80], [81].

Thus, it is critical to find the optimum route while synthesizing a perovskite in order to acquire the best efficiency.

In this chapter, we investigated the effect of different reaction parameters starting with the reaction time, moving to the cesium oleate concentration, and ending with the lead bromide concentration effect.

B. Methods of preparation

Physical properties such as the size and shape depend intensely on the reaction parameters. For this reason, the reaction parameters were optimized in order to prepare the most stable lead bromide perovskites. For this purpose, different reaction times were studied, the concentration of lead bromide was established, and finally the concentration of cesium oleate was also investigated.

1. Effect of reaction time

In this step, 4 different solutions were prepared. Each solution contained 0.08 g lead bromide and was prepared using the same preparation method mentioned in chapter 1. Hence, in this part the addition of cesium oleate was done at 4 different times; once the lead bromide was dissolved ($t=0$ minutes), after 10 minutes; 20 and 40 minutes of dissolving. After that, the solutions were centrifuged; the precipitate was dissolved in hexane and then characterized.

2. Effect of cesium oleate concentration

After choosing the adequate reaction time, the effect of cesium oleate concentration was investigated. So, 4 solutions were prepared by dissolving 0.08 g of

lead bromide in 5 mL octadecene and the synthesis was continued as described in chapter 1. Then, different volumes of cesium oleate (0.4 mL, 0.8 mL, 1.2 mL and 2 mL) were added to the mixture of lead bromide. Thus, 4 solutions were prepared having different concentrations equal to 0.0034 M, 0.0065 M, 0.0092 M and 0.0138 M respectively. After that, the solutions were centrifuged; the precipitate was dissolved in hexane and then characterized.

3. Effect of lead bromide concentration

The final effect that was established was the effect of lead bromide concentration. Consequently, 4 solutions were prepared by dissolving different masses of lead bromide (0.04 g, 0.08 g, 0.15 g and 0.2 g) in 5 mL ODE and the synthesis was continued as described in section 2.3. Thus, 4 solutions were prepared having concentrations of 0.01816 M, 0.0363 M, 0.06812 M and 0.09082 M respectively. After that, the solutions were centrifuged; the precipitate was dissolved in hexane and then characterized.

C. Results and discussion

In our synthesis, three essential solvents were used. In the beginning, oleylamine (OAm) was used as a capping ligand of Pb^{2+} which reduces its reactivity. It strongly coordinates to the Pb ions, and binds to the different facets of CsPbBr_3 which leads to an anisotropic and one-dimensional crystal growth, producing perovskite nanoparticles.

Henceforward, oleic acid (OA) was used as a surfactant playing the role of a protection ligand along with OAm. It also enhances the growth rate of the nanocrystals and controls its size. Finally, octadecene was considered as a noncoordinating solvent; it

is the precipitation medium which induces the perovskite lattice formation. Therefore, it is a good manner to evaluate the effect of the reaction time, and the concentration of both cesium oleate and lead bromide.

1. Optimization of the reaction parameters

The preparation of CsPbBr₃ perovskites was carried out through one simple synthesis route by hot injection method. Hence, many shapes and sizes could be obtained when varying the reaction parameters. Therefore, different optimizations were established, and the obtained perovskites were compared and characterized through XRD, TGA, SEM, UV-Vis and Fluorescence spectroscopy.

a. Reaction time

Four different solutions of lead bromide were prepared. Once lead bromide is dissolved, cesium oleate is added at 4 different times: $t = 0, 10, 20$ and 40 minutes.

According to Gruijter et al., PbBr₂ precursor crystals showed a peak at 330 nm ($S_0 \rightarrow P_1$ transition) [82]. However, the absorption of PbBr₂ perovskites appears at ~ 475 nm as shown in Figure 3A. Thus, the identification of absorption ~ 475 nm makes it easier for establishing the formation of the perovskites in the solution. The absorption peak at 475 nm remained constant with the increase in the reaction time. These results were similar to the one established by Belarbi et al. where it was found that perovskites prepared from PbBr₂ show no significant shift over different reaction times [83].

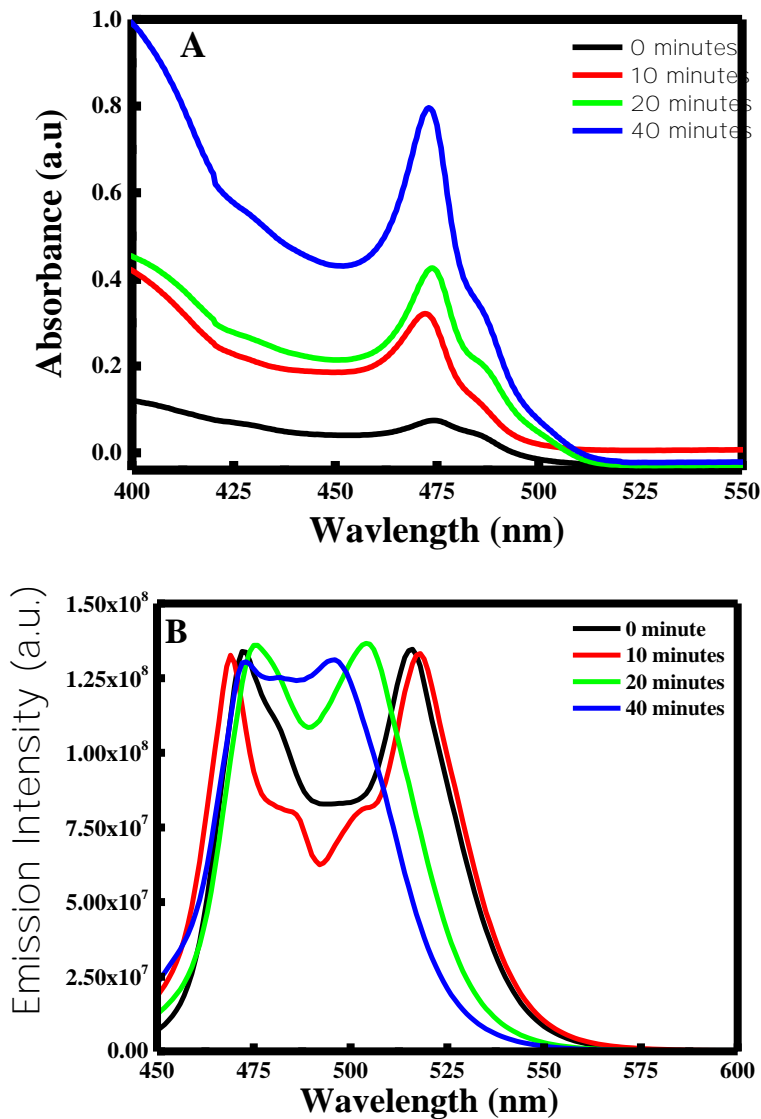


Figure 3 (A) UV-Visible spectra and (B) fluorescence emission spectra of lead bromide perovskites having different reaction times.

Thus, the main difference between the different reaction times was observed in the absorbance value. It is noticeable that the absorbance increases as the reaction time increases. Hence, the highest absorbance was obtained when cesium oleate was added after 40 minutes. Meaning that, the formation of lead bromide perovskites is higher when the reaction is heated for longer time. This can be due to fact that, with time

maximum quantities of lead bromide molecules are being combined to OAm and OA, inducing the enhancement of CsPbBr₃ yield.

Moreover, the successful production of perovskites was verified through the fluorescence emission spectra. The maximum emission peak of lead bromide perovskites was proved to be around 500 nm. Changing the reaction times showed a variation in the emission maxima position and a blue shift of the emission peak was reported with the significant decrease in the crystal size [83]. These changes were very clear in Figure 3B.

In fact, for the different reaction time, 2 distinctive peaks were obtained (See Table 1), where a blue shift appeared during time. The presence of 2 separate peaks reveals the presence of two different components in solution. Hence, according to Fang et al. the peak obtained at a lower wavelength is attributed to the pure PbBr₂, thus the peak obtained at a higher wavelength is attributed to the pure CsPbBr₃ [84].

Time (minutes)	λ_1 (nm)	λ_2 (nm)
0	472	518
10	472	518
20	472	504
40	472	500

Table 1 Emission wavelength of PbBr₂ and CsPbBr₃ at different time.

For the different times the peak at 472 nm remains constant, verifying its attribution to the pure PbBr₂. It is clear that after 40 minutes, the two peaks are being additive to form one broad peak. This change in the peak's shape verifies the complete reaction of PbBr₂ in solution with cesium oleate in order to form fine and small CsPbBr₃ NPs. Hence, the blue shift of the emission intensity wavelength is related to the NPs size. In other words, as a blue shift occurred; smallest NPs are formed. This statement was proved by SEM analysis. Indeed, clear differences in the crystal

morphology were observed. As shown in Figure 4A-D, when the reaction time increases, particles size decreases. These results indicate that 40 minutes are needed to have a complete reaction and to synthesize the smallest perovskites. Although, for $t = 0$ and 10 minutes, large NPs were formed (See Figure 4A&B). Thus, when reaching 20 minutes the CsPbBr_3 start to be formed in smaller size and tends to be more uniform (See Figure 4C). However, at 40 minutes, small and uniform CsPbBr_3 nanoparticles were obtained (See Figure 4D) confirming the peak shapes obtained in the fluorescence emission intensity analysis.

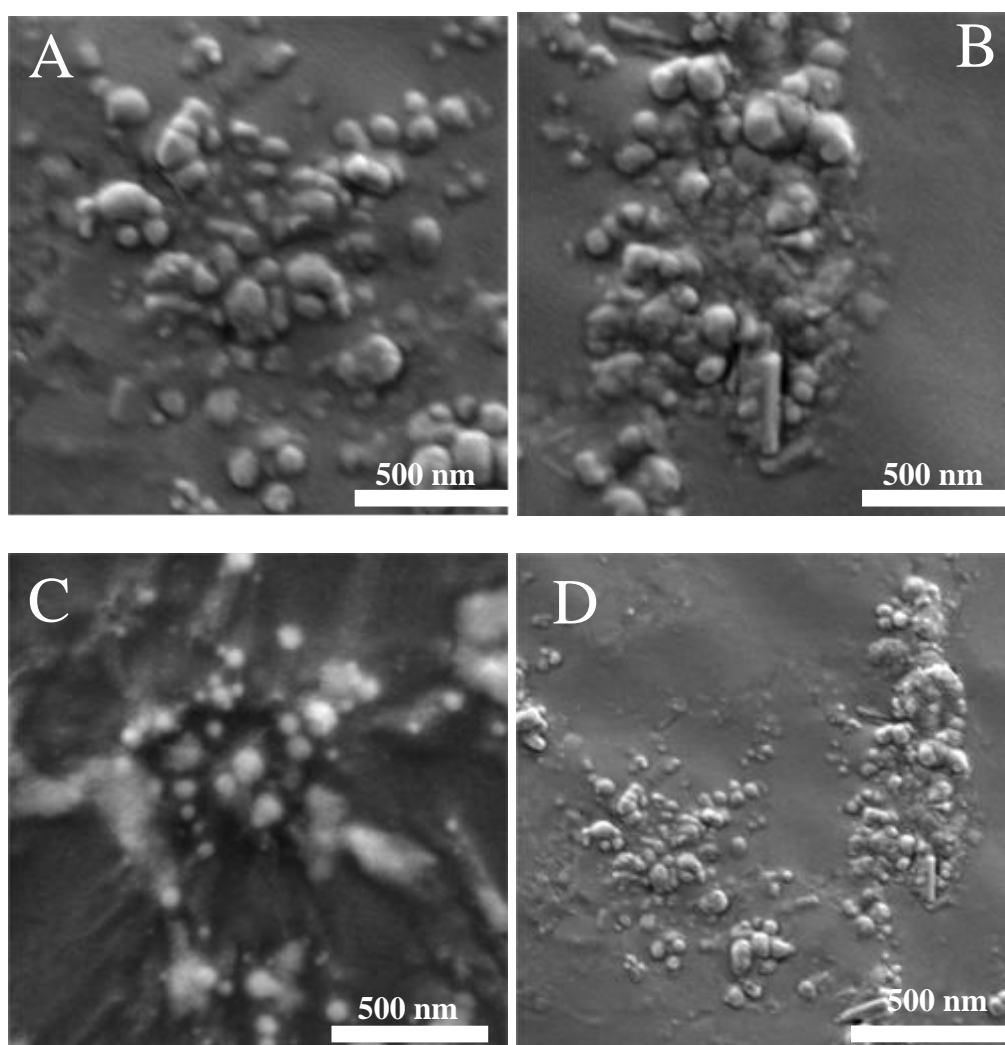


Figure 4 SEM images of lead bromide perovskites at (A) 0 min; (B) 10 min(C) 20 min; and (D) at 40 min.

b. Concentration of cesium oleate

In this part, four different solutions of lead bromide were prepared in order to add different volume of Cs-oleate (0.4 mL, 0.8 mL, 1.2 mL and 2 mL). Thus, the mass of Cs-oleate was (7.53 mg, 15.07 mg, 22.60 mg and 37.66 mg) respectively. Hence, Cs-oleate was added after 40 minutes to ensure that all the PbBr_2 was reacted with OAm and OA.

It is important to mention that, when adding 37.66 mg of cesium oleate, the reaction did not occur and a pale white-yellow color appeared after centrifugation, meaning that cesium oleate is in excess and inhibited the formation of CsPbBr_3 (See figure 5). Thus, the comparison was done for the three remaining experiments having concentrations equal to 0.0034 M ($V=0.4$ mL, $m=7.53$ mg), 0.0065 M ($V=0.8$ mL, $m=15.07$ mg) and 0.0092 M ($V=1.2$ mL, $m=22.60$ mg), respectively.

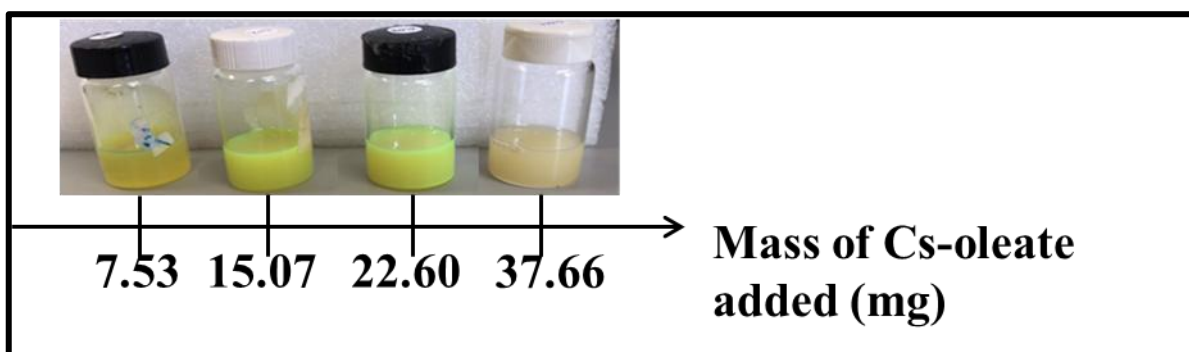


Figure 5 Color change of CsPbBr_3 solution with the increase of Cs-oleate concentration

As reported in the literature, the absorption in the visible region is characteristic of the CsPbBr_3 with an absorption edge at wavelength below 550 nm [85]. According to the results obtain in Figure 6A, as the volume of cesium oleate increases; a slight red shift is obtained from 473 to 477 nm. Hence, this minimal shift has no remarkable effect of the size of the NPs. In consequence, the absorbance value increases as we increase

the volume of cesium oleate. Meaning that, the reaction of PbBr_2 with Cs-oleate increases proportionally, inducing therefore the formation of higher amount of CsPbBr_3 NPs. These results were in accordance with the results obtained with Shi et al [86].

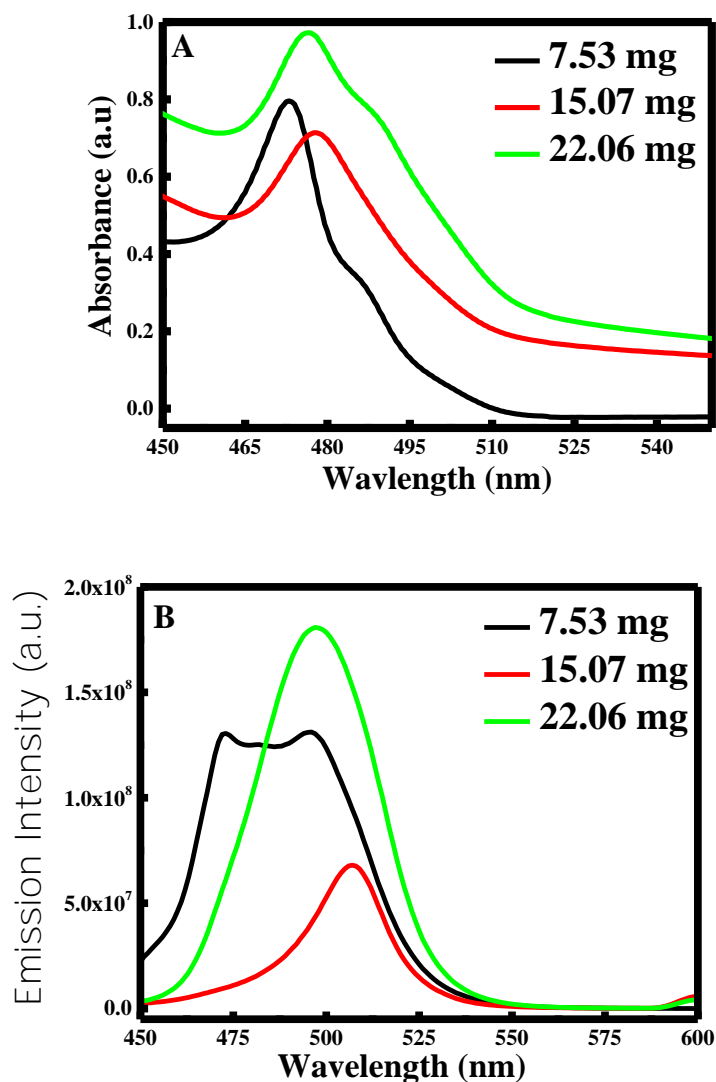


Figure 6 (A) UV-Visible spectra; and (B) fluorescence emission spectra of lead bromide perovskites after adding different masses of cesium oleate.

Remarkably, as shown in Figure 6B, when adding 15.07 mg of Cs-oleate a sharp peak was obtained at 495 nm. Similarly, the same peak was obtained when adding 22.60 mg of Cs-oleate with higher emission intensity; around ~4 fold enhancements.

Thus, a broad peak was obtained when adding a small quantity of Cs-oleate (7.53 mg). These results indicate that an excess amount of Cs-oleate (22.60 mg) is needed to ensure the complete reaction of PbBr_2 with Cs-oleate in order to produce pure CsPbBr_3 NPs. It is important to mention that, the decrease in the emission intensity when adding 15.07 mg compared to the emission intensity when adding 7.53 mg of cesium oleate is due to the complete absence of PbBr_2 in the solution.

Furthermore, SEM analysis was conducted in order to confirm the difference between the three different NPs. As shown in Figure 7A-C, the increase in the Cs-oleate volume encourages the formation of small, fine and uniform NCs. Hence, the particle size decreases from 70-80 nm when adding 7.53 mg and 15.07 mg of Cs-oleate (See figure 7A&B) to 10-20 nm when adding 22.60 mg Cs-oleate (see figure 7C).

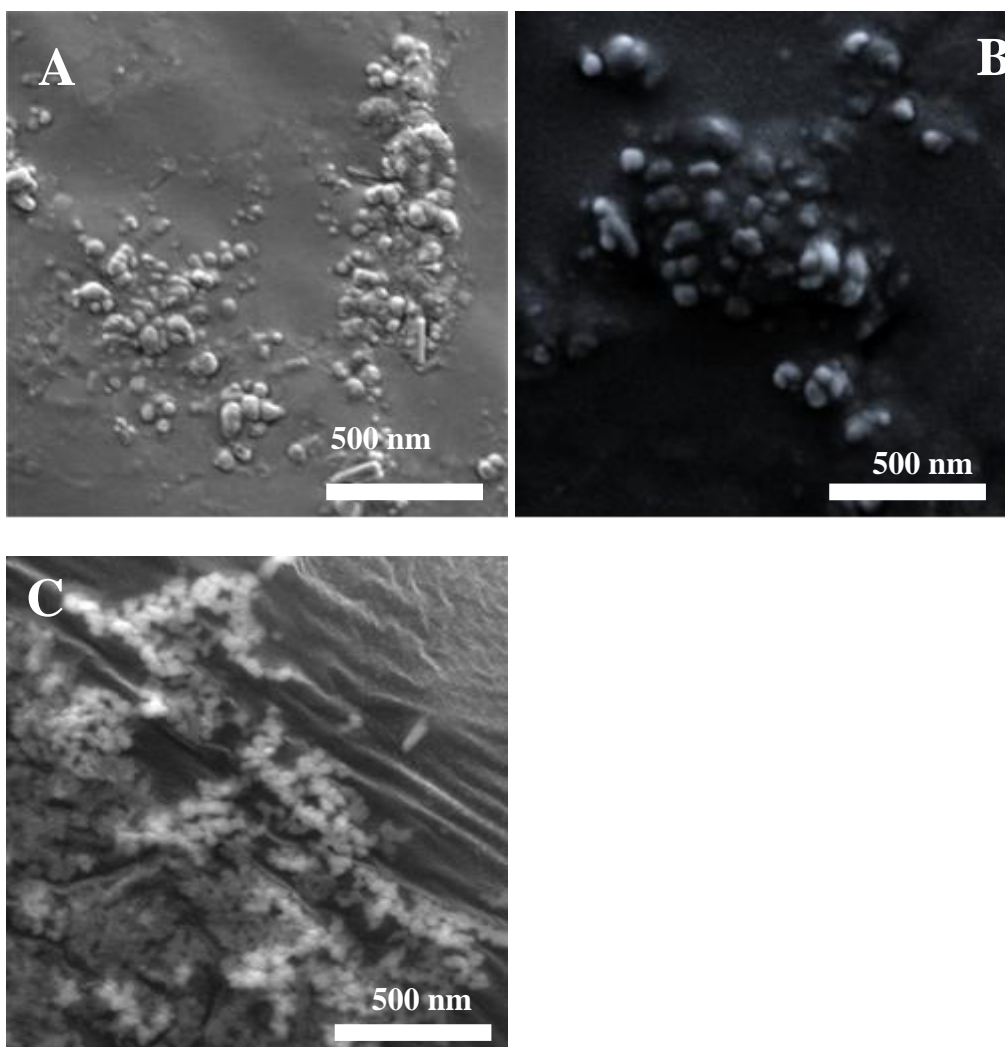


Figure 7 SEM images of lead bromide perovskites with different masses of cesium oleate (A) 7.53 mg; (B) 15.07 mg; and (C) 22.60 mg.

c. Concentration of lead bromide

In order to investigate the effect of lead bromide concentration, 4 different solutions were prepared by varying the mass of PbBr_2 from 0.04 to 0.08 g, 0.15 g and 0.2 g. After 40 minutes, 1.2 mL of cesium oleate was added and the final solution was centrifuged at 15 000 rpm for 15 minutes.

Interestingly, when adding 0.04 g of lead bromide the reaction did not occur, where after centrifugation, no precipitate was formed (See Figure 8). Thus, the comparison and the characterization were done for the remaining experiments (0.08 g,

0.15 g, and 0.2 g) having concentrations equal to 0.0363 M, 0.06812 M and 0.09082 M, respectively.

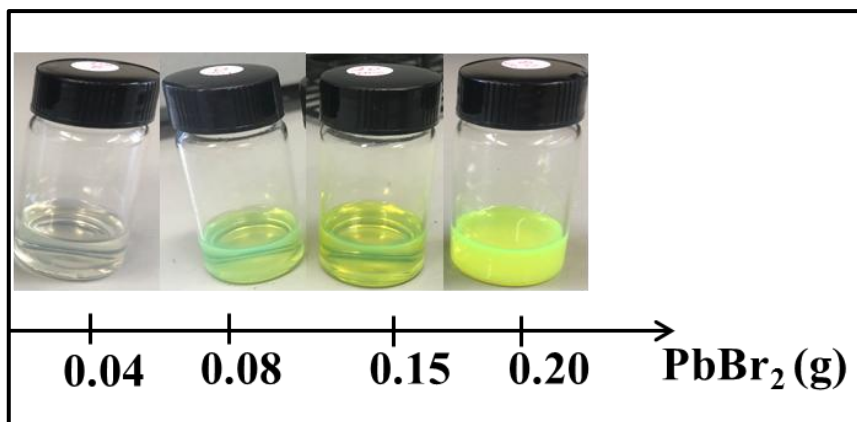


Figure 8 Color change of CsPbBr₃ solution with the increase of lead bromide concentration

Generally, the enhancement of the lead precursor concentration, boost the formation of CsPbBr₃ NPs. Hence, when increasing the mass of PbBr₂ from 0.08 g to 0.15 g, the absorbance increases proportionally, meaning that cesium lead bromide perovskites are being formed, and the yield is increasing with enhanced crystallization (See Figure 9A). However, the absorbance decreases again when adding 0.2 g of lead bromide with a broadening peak. This change in the peak is due to the fact the lead bromide is present in excess in the solution with the CsPbBr₃. These results were proved when measuring the emission intensity, where 2 distinctive peaks were obtained when 0.2 g of PbBr₂ were added (See Figure 9B). Hence, the emission intensity of both CsPbBr₃ when adding 0.08 and 0.15 g was slightly enhanced, proving that 0.15 g are enough to have a maximum yield of CsPbBr₃ NPs.

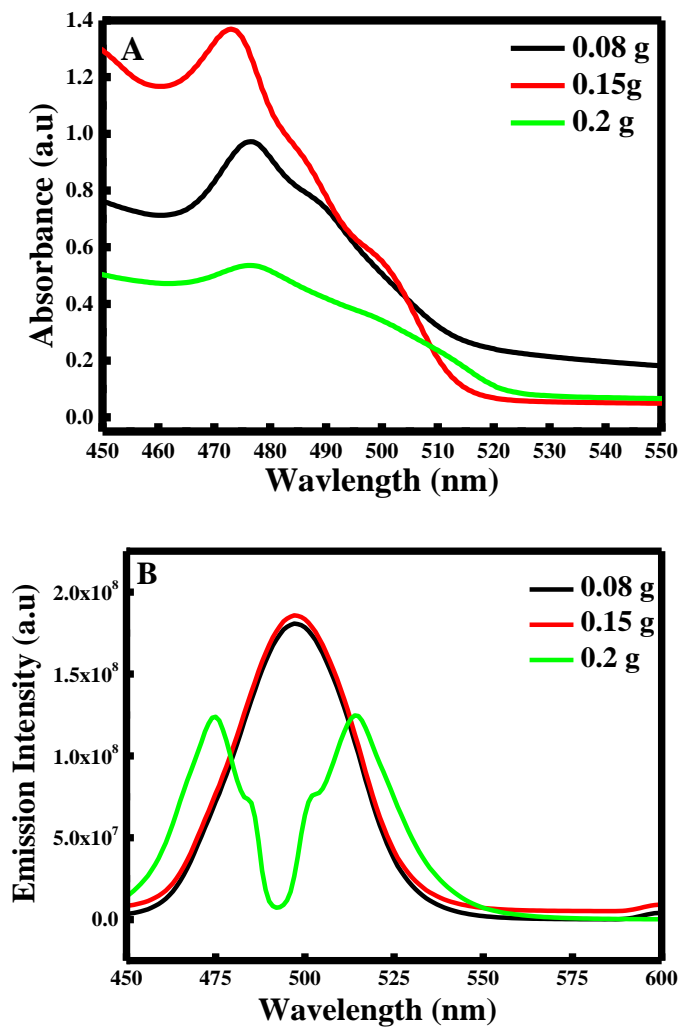


Figure 9 (A) UV-Visible spectra and (B) fluorescence emission spectra of lead bromide perovskites using different masses of lead bromide.

Finally, SEM images were presented in Figure 10A-C, where the NPs increases in size when adding 0.2 g of PbBr_2 and remain the same when adding 0.08 and 0.15 g of the lead precursor.

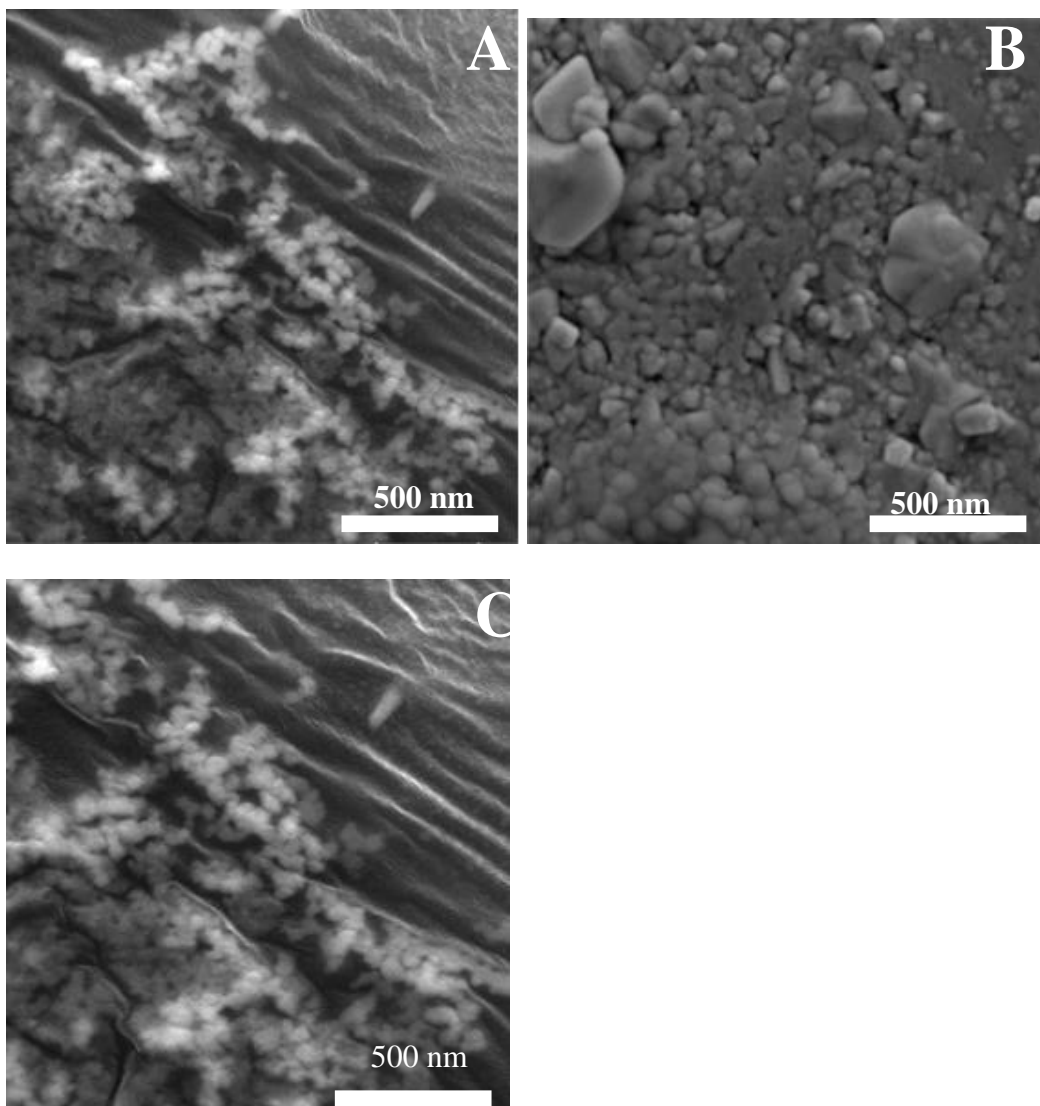


Figure 10 SEM images of lead bromide perovskites having different masses of lead bromide (A) 0.08 g; (B) 0.15 g; and (C) 0.2 g.

2. *Crystallinity analysis of lead bromide perovskites*

To sum up, the best CsPbBr₃ NPs were obtained when mixing after 40 minutes, 0.15 g of PbBr₂ with 1.2 mL of Cs-oleate. To further establish the physical properties of the synthesized perovskites, lead bromide and the synthesized CsPbBr₃ were analyzed by X-Ray Diffraction (XRD) technique. The diffractograms are illustrated in Figure 11.

The main characteristic peaks of lead bromide appeared at diffraction angles of $2\theta^\circ$ equal to 17.49° , 22.919° , 24.833° , 26.111° , 27.82° , 34.045° , 35.405° , 39.041° , 39.75° , 40.602° , 42.597° , and 43.075° [87]. Yet, as it is shown in the diffractogram of the synthesized nanoparticles, these peaks were completely absent. Hence, this confirms the formation of CsPbBr_3 perovskites.

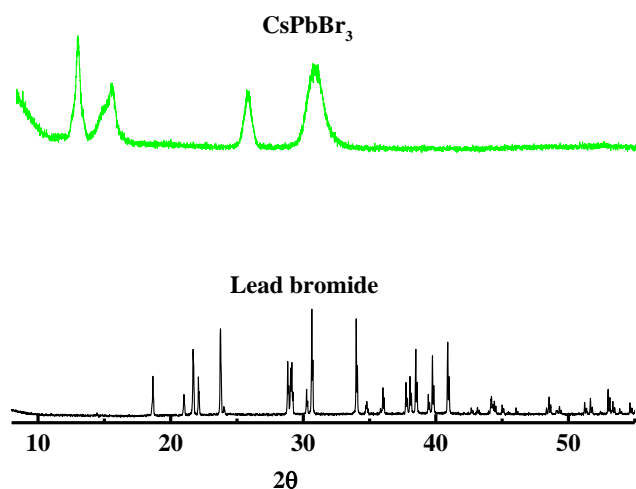


Figure 11 X-Ray Diffractogram pattern of CsPbBr_3 prepared using the optimized method and lead bromide precursor.

Moreover, the XRD pattern of CsPbBr_3 was studied by Boote et al. [88], where the results showed that CsPbBr_3 presents several diffraction peaks at 2θ equal to 15° , 15.2° , 30.4° , and 30.7° . Similar results were obtained for the CsPbBr_3 prepared in our conditions. Besides, 3D CsPbBr_3 and 2D CsPb_2Br_5 structures were studied by Acharyya et al. [89]. The obtained XRD diffractograms proved that if the solution is kept on heating after the addition of cesium oleate, the 3D structure of CsPbBr_3 will be relaxed and transformed into the 2D structure. However, if the solution is directly quenched after the addition of cesium oleate, the 3D structure will be maintained. Hence, the

formed CsPbBr₃ were present in 3D structure, similar to the results obtained by Acharyya et al. [89].

D. Conclusion

In conclusion, CsPbBr₃ were synthesized through a simple method by hot-injection process. It was found that the most stable and smallest CsPbBr₃ NPs were formed when 1.2 mL of cesium oleate was added in the presence of 0.15 g of PbBr₂ for 40 minutes. Moreover, the formed NPs were present in 3D structure with moderate stability.

CHAPTER IV

ENHANCEMENT OF THE STABILITY AND PHOTOLUMINESCENCE QUANTUM YIELD OF CESIUM LEAD BROMIDE PEROVSKITES BY HEXADECYLTRIMETHYLAMMONIUM BROMIDE DOPING

A. Introduction

Metal halide perovskites ($MPbX_3$) have emerged as a new class with extraordinary optical and electronic properties. Halide perovskites are a potential class of materials for photovoltaics, light emitting diodes, lasers, and optical sensors, among other applications. Their major contribution is in solar cells which is due to their high conversion efficiency. Indeed, perovskites have a flexible bandgap and thus they can be tuned to respond to a wide range of colors in the solar spectrum [90].

Generally, metal halide perovskites show numerous benefits in solar cell construction; especially when used as sensitizers where they absorb incident light and supply transport materials with excited carriers [91], [92]. Additionally, they can also act as electron or as an hole transporters depending on the device structure, or even vehicle both charge carriers through bulk perovskite layer, confirming the collection at respective electrodes [93]–[95]. The photoluminescence quantum yield (PLQY) is one of the most essential photophysical properties of perovskites for optoelectronic and solar cell applications.

Though inorganic cesium lead halide ($CsPbX_3$) perovskites have great potential in solar cell applications, the major serious pitfalls of these materials are that they degrade rapidly when exposed to ambient conditions with moderate humidity [69]. Not only do extrinsic factors such as moisture, temperature, UV light, electric field and

oxygen cause the degradation of perovskites [96], but also intrinsic factors such as ion migration in the vacancies of the perovskites' structure [97]. These limitations have induced the increased study of the addition of surfactants to enhance their stability. The ligand doping strategy, through the partial substitution of foreign ions for native ions, has gradually become an effective method for significantly enhancing the comprehensive properties of CsPbBr₃.

In this chapter, the addition of CTAB was established in order to increase the stability and PLQY of the prepared CsPbX₃ perovskites.

B. Methods of synthesis

1. Preparation of CTAB solution

CTAB solution was prepared by mixing 0.05 g hexadecyltrimethylammonium-bromide with 10 mL ODE and 0.62 mL OA into a vial. The solution was stirred and heated at 200^oC until complete dissolution of CTAB and the color turned from transparent to yellow. The resultant solution was sealed and stored at room temperature for further use.

2. Effect of CTAB

After choosing the adequate reaction time, concentrations of lead bromide and cesium oleate (from Chapter III), the effect of CTAB was expanded. And so, a solution was prepared as mentioned in chapter II until the complete dissolving of PbBr₂ in solution. Later, 1 mL of CTAB solution was added followed by the addition of 1.2 mL of Cs-oleate and another addition of 1 mL of CTAB solution. Then, the solution was

immediately immersed in a cold-water bath ($T= 10^{\circ}\text{C}$). Finally, the solution was centrifuged, and the precipitate was dissolved in hexane.

C. Results and discussion

1. Photoluminescence stability of CsPbBr₃ in the presence and absence of CTAB

The fluorescence emission spectrum of the prepared solutions was measured for different times in order to access the photoluminescence (PL) stability of the perovskites in the absence and presence of CTAB. As shown in Figure 12A&B the emission intensity of CsPbBr₃ decreases gradually within time in the presence and absence of CTAB. However, after 24 hours, the PL intensity of the prepared CsPbBr₃ in the presence of CTAB remains almost constant, whereas the PL intensity for the NPs prepared without CTAB decreases consistently. The difference in the PL intensity in the absence and presence of CTAB is remarkable when plotting I/I_0 vs time as depicted in Figure 12C.

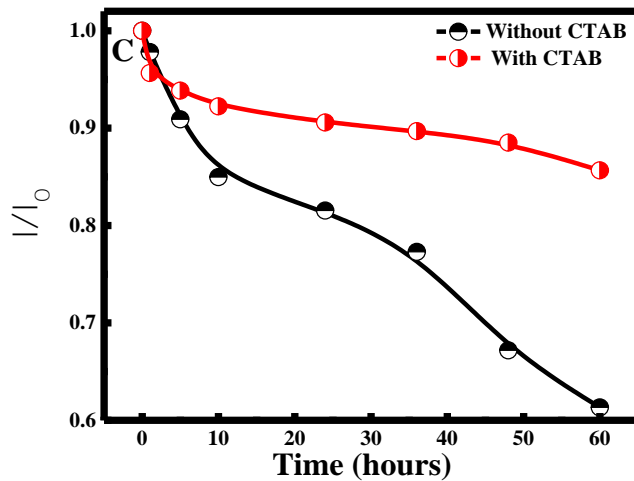
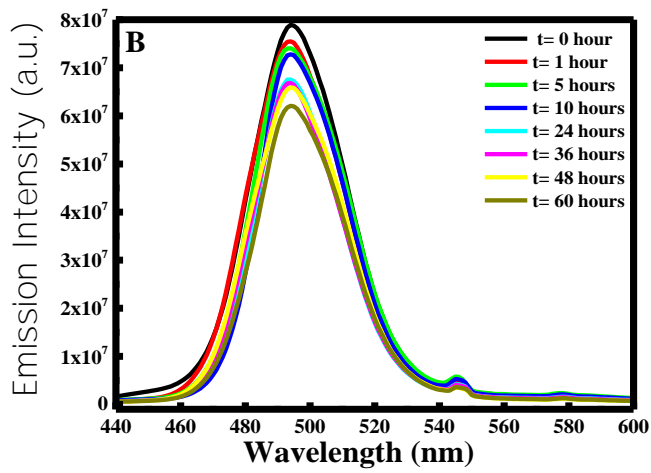
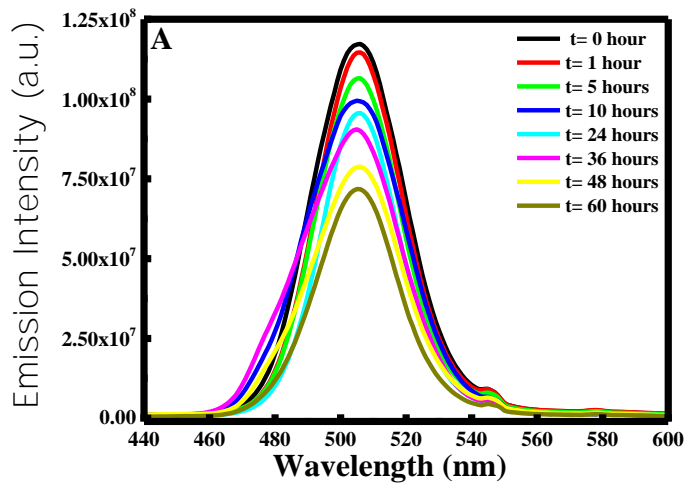


Figure 12 Fluorescence emission intensity of CsPbBr₃ (A) in the absence of CTAB; (B) in the presence of CTAB; and (C) the plot of I/I_0 for CsPbBr₃ in the absence and presence of CTAB within time from 0 to 60 hours.

Similar pattern was observed according to Liu et al, where the CsPbBr₃ perovskites lost 62 % of their PL intensity after 4 days [98]. Obviously, the decrease was rapid for the solution lacking CTAB, where the PL intensity decreases by around ~40%. However, this loss was slower for the solution containing CTAB where the PL intensity of CsPbBr₃ decreases only by ~15% after the same period of time.

Remarkably, as shown in Figure 13, after 60 hours, the PL intensity of CsPbBr₃ increases, complemented with a peak split into 2 distinctive peaks. In fact, the presence of 2 separate peaks reveals the presence of two different components in solution. As proved earlier, according to Fang et al. the peak obtained at a lower wavelength is attributed to the pure PbBr₂ [84]. This proves that CsPbBr₃ perovskites were degraded and the PbBr₂ precursor was free again in the solution. Interestingly, in the presence of CTAB, the shape of the PL intensity peaks remains unchanged (See Figure 13). Thus, the incorporation of PbBr₂ inside the perovskites was maintained by enhancing their stability in the presence of CTAB.

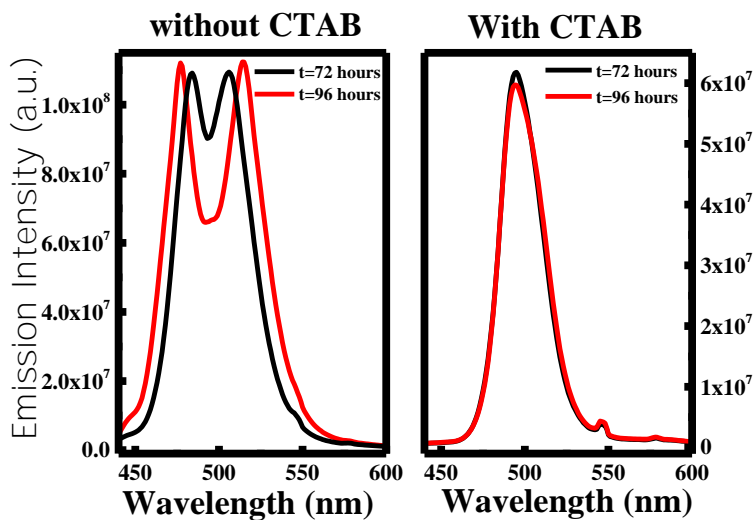


Figure 13 The difference in the shape of PL intensity peaks in the absence and the presence of CTAB after 60 hours.

2. Thermal stability of CsPbBr₃ in the presence and absence of CTAB

Thermogravimetric analysis was performed to assess the stability of the prepared nanoparticles. As shown in Figure 14, PbBr₂ totally loses its mass upon reaching a temperature slightly below 700°C. However, no mass loss was occurred between 100 °C - 400 °C. Yet, for both CsPbBr₃ prepared in the absence and in the presence of CTAB, almost 10% of their mass was lost. Hence, this mass loss is initially related to the presence of hexane. Henceforth, the weight loss of CsPbBr₃ in both cases occurred at 450 °C, similar to pure PbBr₂. Thus, CsPbBr₃ prepared without CTAB loses around 40 % of its mass. Moreover, the weight loss was proved to be due to the removal of the capped alkyl amines at low temperatures and the sublimation of PbBr₂ at high temperatures [89]. Hence, this degradation pattern was identical to the TGA analysis done by Xu et al. [99]. This difference in the degradation pattern of the 2 components means that PbBr₂ inside the perovskite is less degraded and is thus more stable.

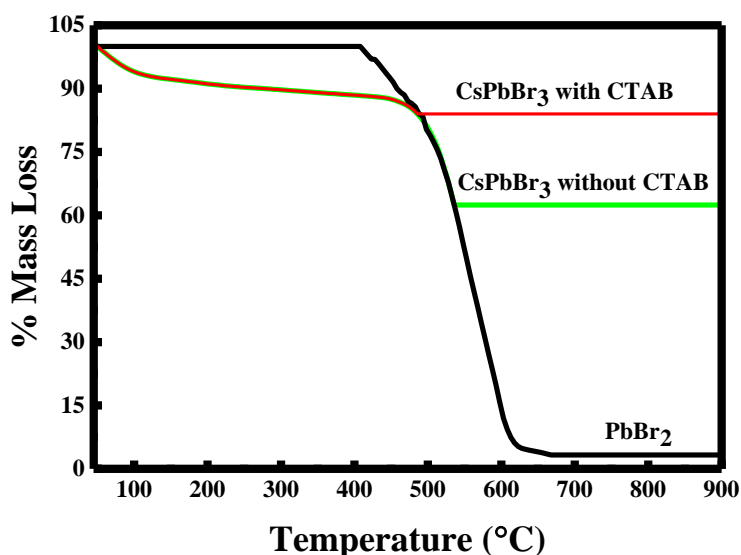


Figure 14 Thermogravimetric analysis TGA of lead bromide perovskites.

Although, the addition of CTAB, decreases the degradation of the CsPbBr₃ and decreases its decomposition, where it loses only 15% of its total mass. Hence, the increase in the thermal stability in presence of CTAB, can be due to the fact that CTAB molecules contain methylammonium groups that enhance the incorporation of PbBr₂ inside the perovskites.

3. Photoluminescence quantum yield in the presence/absence of CTAB

The reference used to determine the Photoluminescence quantum yield was quinine sulfate dihydrate having $\Phi = 0.546$ and an emission range of 400-600 nm. The synthesized CsPbBr₃ were analyzed by Fluorimetry technique at 200 °C and 40 °C in the absence of CTAB. The results are depicted in Figure 15.

According to the plotted data, for both temperatures, the highest quantum yield was obtained when cesium oleate was added after 40 minutes, meaning that the formation of lead bromide perovskites is higher when the reaction is heated for longer time. As proved earlier, this is due to fact that within time, maximum quantities of lead bromide molecules are being combined to OAm and OA, inducing the enhancement of CsPbBr₃ yield.

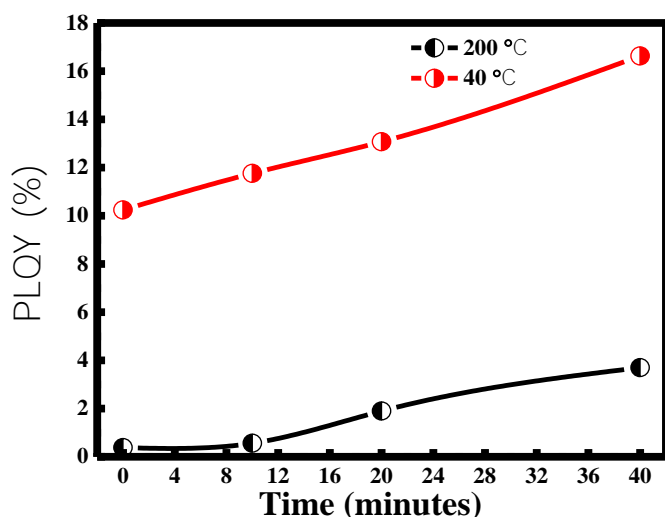


Figure 15 PLQY (%) of CsPbBr₃ in the absence of CTAB at 40°C and 200°C

Moreover, decreasing the temperature from 200°C to 40°C has shown a remarkable effect on the PLQY values. In fact, according to Thomson et al., the % of PLQY decreases nonlinearly as the temperature increases, where the value of PLQY increases from 0.02 % at 200K and reached a maximum of 0.43 % at about 80K [100]. Similar pattern of PLQY values was obtained when decreasing the temperature to 40°C.

Hence, upon lowering the temperature from 200°C to 40°C, the PLQY increases from 3.7% till 16.63 % for t=40 minutes. Therefore, at 40 °C, the PLQY of CsPbBr₃ increased remarkably over 4 times, higher than the values obtained at 200 °C (see table2).

	PLQY (%)	
Time (min)	40 °C	200 °C
0	10.24	0.38
10	11.76	0.56
20	13.07	1.9
40	16.63	3.7

Table 2 PLQY % of CsPbBr₃ at different time and temperature.

This increase in PLQY while decreasing the temperature; was proved to be due to the immobility of the charge carriers at low temperatures, and thus their inability to reach the non-radiative recombination centers. As temperature decreases, the immobile charge carriers will combine radiatively and thus increase PLQY % [100].

Moreover, the effect of CTAB was established on the PLQY values and the results were depicted in Figure 16.

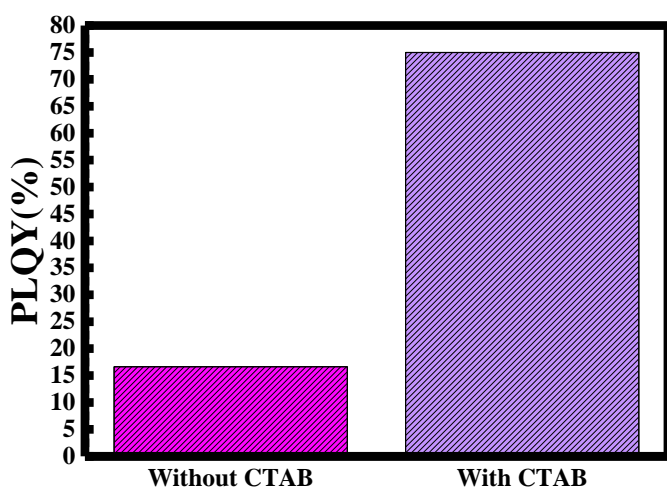


Figure 16 PLQY variation in the presence and the absence of CTAB.

Interestingly, the PLQY % of CsPbBr₃ was enhanced to reach ~75% when CTAB was added to the solution. It is remarkable that the presence of CTAB boosts the PLQY ~4 fold. This increase is due to the enhancement of the stability of the synthesized perovskites upon the addition of CTAB related to the presence of methylammonium groups. Different PLQY values found in the literature were listed in Table 3.

Perovskites prepared	PLQY (%)	References
CTAB-mediated antisolvent vapor route to shalelike Cs_4PbBr_6 microplates	59	[101]
CsPbBr ₃ Nanocrystal Solid-State Films	54	[102]
Bismuth-Doped Hybrid Lead Bromide Perovskite Nanocrystals	64	[103]
methylammonium lead bromide/formate mixture	69	[104]
CTAB dopped CsPbBr ₃	75	Our work

Table 3 Different PLQY values obtained in the literature

D. Conclusion

In conclusion, it was verified that the addition of CTAB is crucial in terms of the increase of the photoluminescence stability, thermal stability and in boosting the PLQY %. In the first place, the addition of CTAB has enhanced the stability of the PL intensity peak of the formed CsPbBr₃, where the PL intensity decreases by only ~15% within 4 days. Furthermore, the presence of CTAB stabilizes the incorporation of PbBr₂ inside the perovskites, where the formed CsPbBr₃ loses only around ~10% of their total mass. Finally, the PLQY was boosted from 16% to 75% in the presence of CTAB.

CHAPTER V

HEXADECYLPYRIDINIUM BROMIDE AS A NEW CAPPING AGENT FOR THE CRYSTAL STRUCTURE PRESERVATION OF CESIUM LEAD BROMIDE PEROVSKITES

A. Introduction

The optical and electronic properties of lead halide perovskites are dependent on their surface defects. Atomic compositions can vary between the interior and surface of perovskite crystals, this results in undesirable quantum states within the energy band gap, which negatively affects the optoelectronic properties and the photoluminescence (PL) stability [105].

The simple fabrication of perovskite thin films by solution process frequently results in various uncontrollable defects, such as uncoordinated Pb cations and halide vacancies which generates non-radiative recombination sites and decreases the photoluminescence quantum yield (PLQY) of the perovskite [106].

Increased research into the addition of a stabilizing surfactant to perovskites was shown to improve quantum yield [107]. For instance, increasing surface passivation via salt solutions [108], generating other cation/anion compositions through doping [109] or post-synthetic ion exchange [110]. Many researchers investigated a method of chemical passivation to minimize defect formation in order to overcome this issue. Ligand exchange at the perovskites' surface stabilizes the perovskite and enhances its PLQY.

In this chapter, Hexadecylpyridinium bromide (CPB) was used as a new capping agent for the crystal structure preservation of CsPbBr₃ perovskites. The addition of CPB was established to preserve the crystal structure of CsPbBr₃ and maintain its strong green photoluminescence (PL) emission.

B. Methods of preparation

1. Preparation of CPB solution

CPB solution was prepared by mixing 0.05 g hexadecylpyridinium bromide with 10 mL ODE and 0.62 mL OA into a vial. The solution was stirred and heated at 200°C until complete dissolution of CPB and the color turned from transparent to yellow. The resultant solution was sealed and stored at room temperature for further use.

2. Effect of CPB/ CTAB

Using the best optimization results, CsPbBr₃ perovskites were prepared as mentioned in chapter II until the complete dissolving of PbBr₂ in the solution. Later on, 1 mL of either CPB or CTAB solution was added followed by the addition of 1.2 mL of Cs-oleate and another 1 mL of either CPB or CTAB solution. The solution was immediately immersed in a cold-water bath (T= 10°C). Finally, the solutions were centrifuged, and the precipitate was dissolved in hexane.

3. Effect of PbI₂

The effect of PbI₂ on the synthesized perovskites is studied. For this reason, PbI₂ solution (0.043 μM) was prepared by dissolving 2 mg lead iodide with 10 mL hot distilled water. Moreover, new samples of cesium lead bromide perovskites were prepared with the addition of either CPB or CTAB. Then, 10 μL of this solution was pipetted, placed on a glass slide, and placed in a vacuum oven at 30° C overnight.

Henceforth, the slide was placed in a cuvette into the fluorometer. The emission spectra were measured while gradually increasing the concentration of PbI₂ (from 0.0072 μM to 0.024 μM).

C. Results and discussion

1. Characterization of CsPbBr₃ perovskites prepared in the presence of CPB and CTAB

To investigate the optical properties of the CsPbBr₃ perovskites prepared using different capping agents, CTAB and CPB, their absorption spectra was measured. As seen in Figure 17A, doped CsPbBr₃ perovskites did not exhibit significant change of the absorption band edge and emission peak position near 475 nm, indicating that the original crystal structure of CsPbBr₃ was essentially unchanged by the capping agents. Thus, the main difference between CPB and CTAB was observed in the absorbance value. The highest absorbance was obtained when CPB was added meaning that the formation of lead bromide perovskites is higher.

Furthermore, the successful production of perovskites was verified through the fluorescence emission spectra. The PL spectra for the synthesized CsPbBr₃ perovskite in the presence of CPB and CTAB are depicted in Figure 17B. Interestingly, the addition of either CPB or CTAB to the CsPbBr₃ perovskite showed significant improvement in PL intensity. The increase of PL intensity at the same emission wavelength is indicative of enhanced radiative recombination. Such enhancement can be attributed to the binding of cetylpyridinium, cetyltrimethylammonium, and bromide ions to the surface defects of the CsPbBr₃ crystals, reducing non-radiative recombination centers, such as uncoordinated Pb cations and halide vacancies [111].

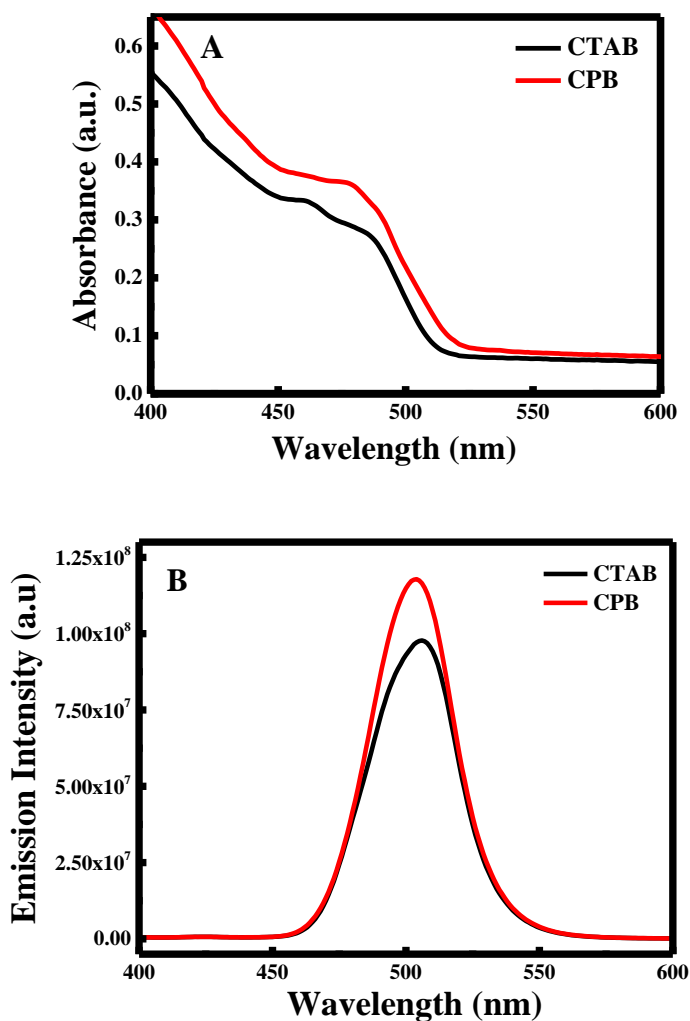


Figure 17 (A) UV-Visible spectra and (B) fluorescence emission spectra of lead bromide perovskites prepared using different capping agents.

Moreover, the maximum emission peak of lead bromide perovskites was proved to be around 500 nm. Thus, the main difference between CPB and CTAB was observed in the PL intensity value. This increase in the intensity upon the addition of CPB confirms that the formation of lead bromide perovskites is higher. However, a very small blue shift is obtained when CPB was added. Hence, the blue shift of the emission

intensity wavelength is related to the NPs size. In other words, as a blue shift occurred; uniform and smallest NPs are formed.

This statement was proved by SEM analysis. Actually, clear differences in the crystal morphology were observed. As shown in Figure 18A-B, when CPB is added, small and uniform CsPbBr_3 nanoparticles were obtained, confirming the sharp peak shapes obtained in the fluorescence emission intensity analysis (See Figure 18A)

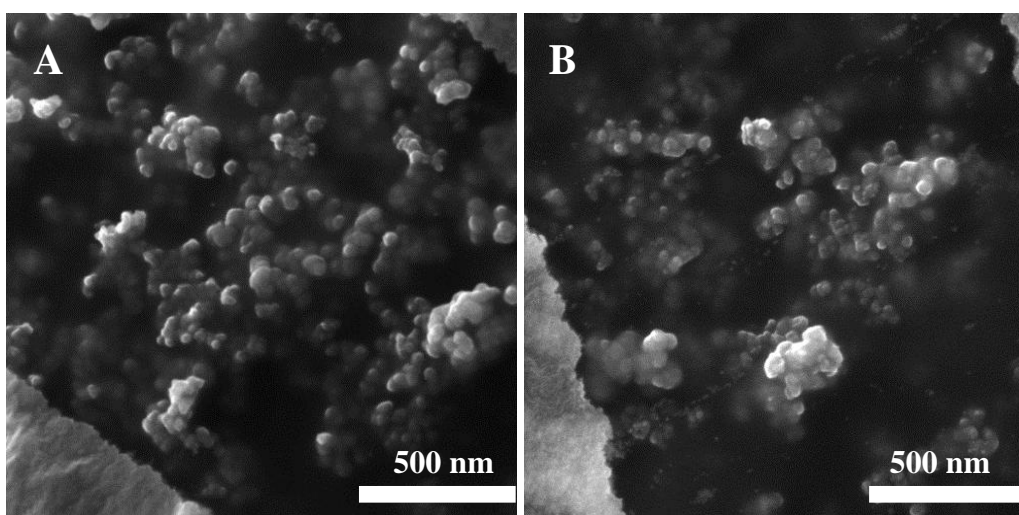


Figure 18 SEM images of lead bromide perovskites with the addition of either (A) CPB or (B) CTAB.

2. Thermal stability of CsPbBr_3 in the presence of either CPB or CTAB

Thermogravimetric analysis was performed to assess the stability of the prepared nanoparticles (See Figure 19). For both CsPbBr_3 prepared in the presence of either CPB or CTAB, almost 10% of their mass was lost. Hence, this mass loss is initially related to the presence of hexane. Henceforth, a slight mass loss around 10% was observed between 100°C – 200°C. This loss is probably due to the removal of oleylamine and

oleic acid. According to Boote et al., lead halide perovskites lose most of their masses in this temperature range due to the presence of oleylamine and oleic acid ligands [88].

Moreover, the weight loss was proved to be due to the removal of the capped alkyl amines at low temperatures and the sublimation of PbBr_2 at high temperatures [89].

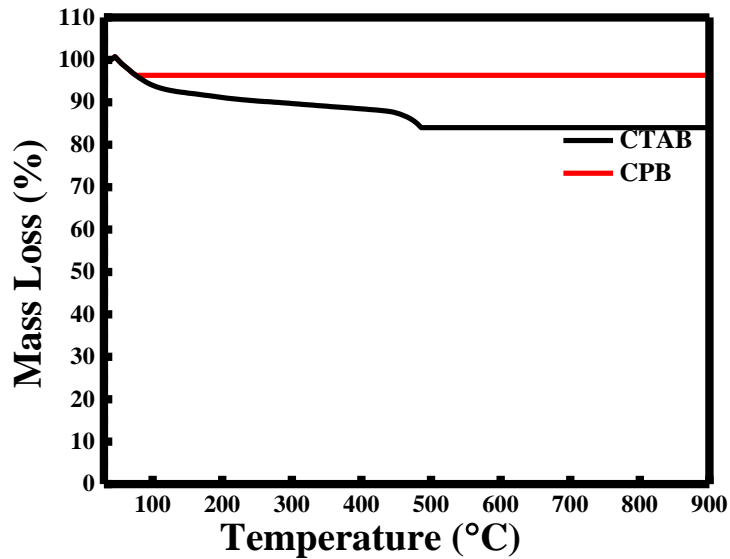


Figure 19 Thermogravimetric analysis TGA of lead bromide perovskites.

This degradation pattern was identical to the TGA analysis done by Xu et al. [99]. This difference in the degradation pattern of the 2 components means that PbBr_2 inside the perovskite is less degraded and is thus more stable. Therefore, the addition of CPB or CTAB decreases the degradation and decomposition of the CsPbBr_3 perovskite. Hence, the increase in the thermal stability in presence of CPB can be due to the fact that CPB pyridinium, enhancing therefore the incorporation of PbBr_2 inside the perovskites.

3. Photoluminescence quantum yield in the presence of CPB and CTAB

Moreover, the effect of CTAB and CPB were established on the PLQY values, and the results were depicted in Figure 20.

The reference used to determine the Photoluminescence quantum yield was quinine sulfate dihydrate having $\phi = 0.546$ and an emission range of 400-600 nm. The synthesized CsPbBr₃ were analyzed by fluorescence emission intensity.

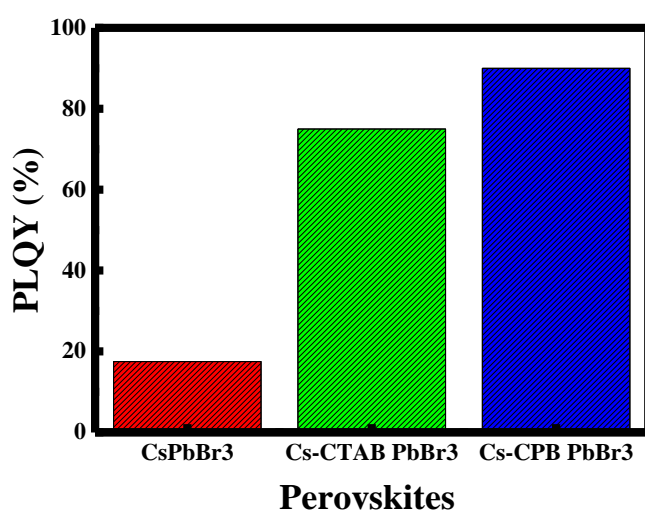


Figure 20 PLQY variation in the presence and the absence of either CPB or CTAB.

Interestingly, the PLQY % of CsPbBr₃ was enhanced to reach ~90% when CPB was added to the solution compared to 75% upon the addition of CTAB and 17% in the absence of any surfactant. This increase is due to the enhancement of the stability of the synthesized perovskites upon the addition of CPB which is related to the presence of pyridinium groups. Different PLQY values found in the literature were summarized in Table 4.

Perovskites prepared	PLQY %	References
methylammonium lead bromide/formate mixture	69	[104]
CsPbBr ₃ Nanocrystal Solid-State Films	54	[102]
CsPbBr ₃ doped with ZnBr ₂ -CPB	30	[112]
CPB doped CsPbBr ₃ perovskites	99	Our work

Table 4 Different PLQY values obtained in the literature.

4. Variation in the photoluminescence of CsPbBr₃ upon the addition of PbI₂ in the presence of either CPB or CTAB

The fluorescence emission spectrum of the prepared solutions was measured in the presence of either CPB or CTAB to access the effect of lead iodide (PbI₂) on the photoluminescence (PL) stability of the perovskites.

According to Figure 21, in both cases, initially the maximum emission peak was around 500 nm. This confirms the successful formation of CsPbBr₃ perovskites. In the presence of CTAB, when adding water, the emission intensity decreases (See figure 21A). Essentially this is due to the dissociation of the CsPbBr₃ perovskite crystal into its ions due to the presence of water. Remarkably, a red shift (from 506 nm to 520 nm) and a continuous decreasing in the emission intensity were obtained when adding PbI₂. This shift and this decreasing confirm the anion exchange between Br⁻ and I⁻ inducing the formation of CsPb[Br/I]₃ perovskites.

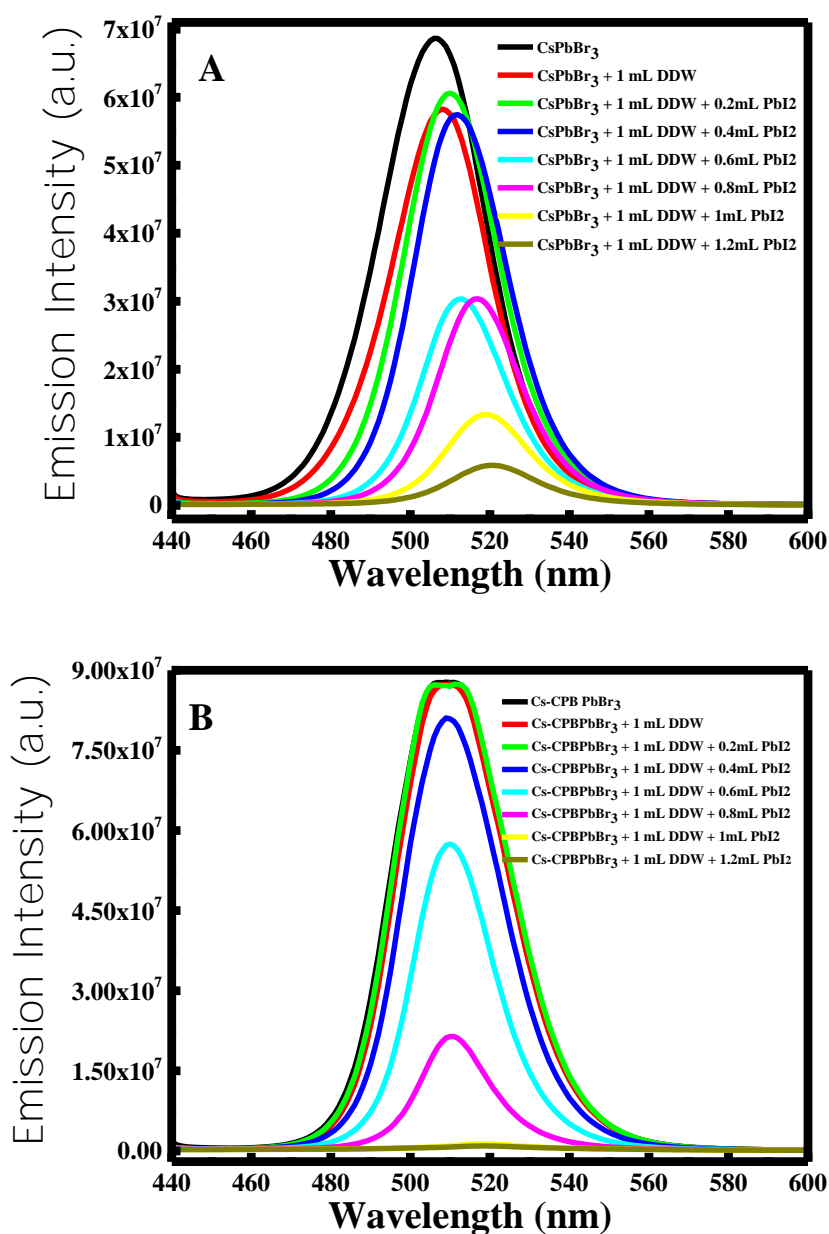


Figure 21 Variation of the fluorescence emission intensity of CsPbBr₃ upon the addition of PbI₂ (A) in the presence of CTAB and (B) in the presence of CPB.

However, in the presence of CPB, it is obvious that when adding water, the emission intensity remains constant (See Figure 21B). Thereby, in the presence of CPB, the lead bromide inside the perovskites was not affected and therefore protected from any other interactions. Henceforward, when adding PbI₂ solution, from (0.2 mL to 0.8

mL), the emission intensity slightly decreases with no remarkable shift. Hence, this is due to the fact that PbI_2 molecules are being attracted to the pyridinium group present in CPB molecules, inducing the formation of CPB- PbI_3 perovskites. Thus, at higher volume of PbI_2 (1 mL and 1.2 mL) a remarkable red shift was obtained (from 509 nm to 520 nm), inducing therefore the penetration of PbI_2 into the perovskites and therefore the formation of Cs-CPB- $[\text{Br/I}]_3$ perovskites. These results confirm the role of CPB as a capping agent in preserving the crystal structure of CsPbBr_3 .

D. Conclusion

In conclusion, CsPbBr_3 were synthesized through a simple method by hot-injection process. It was verified that CPB was a better stabilizing agent than CTAB due to the attachment of cetylpyridinium and bromide ions to the surface defects of the CsPbBr_3 crystals. Moreover, a huge number of small and uniform CsPbBr_3 NPs were formed upon the addition of CPB. Furthermore, the presence of CPB causes the increase in the thermal stability of CsPbBr_3 due to the presence of pyridinium groups respectively that enhance the incorporation of PbBr_2 inside the perovskites. Henceforth, the addition of CPB boosted the PLQY to 90%. Finally, CPB acts as a capping agent in preserving the crystal structure of CsPbBr_3 and preventing the anion exchange between bromide and iodide ions upon the addition of low concentrations of PbI_2 .

CHAPTER VI

CESIUM LEAD IODIDE PEROVSKITES IN THE PRESENCE OF CTAB LIGAND FOR HIGHER TIME STABILITY AND BETTER PHOTOLUMINESCENCE QUANTUM YIELD

A. Introduction

Despite the various techniques that can offer fine perovskites; the synthesis of stable cesium lead iodide perovskites remains an actual challenging field. Indeed, cesium lead iodide perovskites (CsPbI_3) are hard to synthesize due to their rapid transformation into different phases. In fact, α - CsPbI_3 perovskites have high absorptivity and high photoluminescence quantum yield which allowed them to gain significant interest in several applications [113]. However, α - CsPbI_3 is only stable at high temperatures above 370°C [114]. At lower temperatures, it is quickly transformed into β -tetragonal and then γ -orthorhombic metastable phases and finally into a non-perovskite yellow δ - CsPbI_3 phase [114]. Although the transformation of α - CsPbI_3 into δ - CsPbI_3 is rapid in presence of moisture and humidity [115]. However, not all α - CsPbI_3 perovskites act in the same manner. Henceforth, large α - CsPbI_3 in the range size between 100-200 nm degrade rapidly, however small colloidal α - CsPbI_3 in the range size between 5-15 nm, might be stabilized at ambient temperature due to the presence of capping agents [116] or also by the partial replacement of iodide with bromide [117].

In our work, the synthesis of cesium lead iodide perovskites was carried out based on the hot injection method using different surfactant ligands to control the synthesis of inorganic perovskite CsPbI_3 nanoparticles. Henceforth, the addition of either CTAB or SiO_2 NPs was established in order to maintain the α - CsPbI_3 phase and increase the stability and PLQY of the prepared CsPbX_3 perovskites.

B. Methods of preparation

Perovskites have been shown to degrade rapidly when exposed to ambient conditions with moderate humidity. Consequently, the addition of a ligand, acting as stabilizing agent is strictly needed to increase the time-dependent stability of the formed perovskites. For this purpose, several solutions were prepared to test in the first place the effect of CTAB-oleate addition, and secondly to test the effect of SiO₂ NPs-oleate solution.

1. Effect of CTAB-oleate solution

In this step, 4 solutions were prepared. Each solution contains 0.08 g lead iodide and prepared using the same preparation method mentioned in section 2.5. After the complete dissolution of lead iodide, CTAB-oleate solution was added in different ways:

- Solution A: 0.4 mL cesium-oleate was added (control experiment).
- Solution B: 0.4 mL cesium oleate was added followed by 1 mL of CTAB-oleate solution.
- Solution C: 1 mL of CTAB-oleate solution was added followed by 0.4 mL cesium oleate and 1 mL of CTAB-oleate solution.
- Solution D: 1 mL of CTAB-oleate solution was added.

After complete reaction, the solutions were immersed in a cold bath, centrifuged and the precipitate was dissolved in hexane.

2. *Effect of SiO₂-oleate solution*

a. Preparation of SiO₂-oleate solution

First, the preparation of colloidal silica nanoparticles was carried out based on Rao *et al.* [118]. Next, 0.1 g of the formed nanoparticles was mixed with 10 mL ODE and 0.62 mL OA into a vial. The solution was stirred and heated at 200°C until complete dissolution of SiO₂ NPs. Similarly, to the CTAB-oleate and Cs-oleate solution, the color of SiO₂ NPs solution turned from transparent to yellow confirming the formation of SiO₂ NPs-oleate. The solution was sealed and stored at room temperature for further use.

b. Preparation of perovskites sample in the presence of SiO₂-oleate solution

Similarly, the effect of SiO₂ NPs-oleate solution was investigated. The samples were prepared as follow:

- Solution A: 0.4 mL cesium-oleate was added (control experiment).
- Solution B: 0.4 mL cesium oleate was added followed by 1 mL of SiO₂ NPs-oleate solution.
- Solution C: 1 mL of SiO₂ NPs-oleate solution was added followed by 0.4 mL cesium oleate and 1 mL of SiO₂ NPs-oleate solution.
- Solution D: 1 mL of SiO₂ NPs-oleate solution was added.

In all the samples 0.08 g of lead iodide were used, and after complete reaction, the solutions were immersed in a cold bath, centrifuged and the precipitate was dissolved in hexane.

C. Results and discussion

1. *Synthesis of lead iodide perovskites*

Initially, lead iodide perovskites were prepared in the presence of cesium oleate only. As shown in Figure 22A, after 40 minutes; before centrifugation; the solution color was red verifying the formation of cesium lead iodide perovskites (CsPbI_3). Remarkably, after centrifugation the color turned to pale yellow in the presence of a yellow precipitate (See Figure 22B). This color change is due to the fact that CsPbI_3 nanoparticles undergo a fast decomposition when exposed to ambient air. Consequently, the synthesis of CsPbI_3 was carried out by adding a capping agent acting as a surfactant (CTAB), in order to increase the stability of the formed perovskites when exposed to ambient air. The synthesis of lead iodide perovskites was established in the presence of either CTAB, or silica nanoparticles.

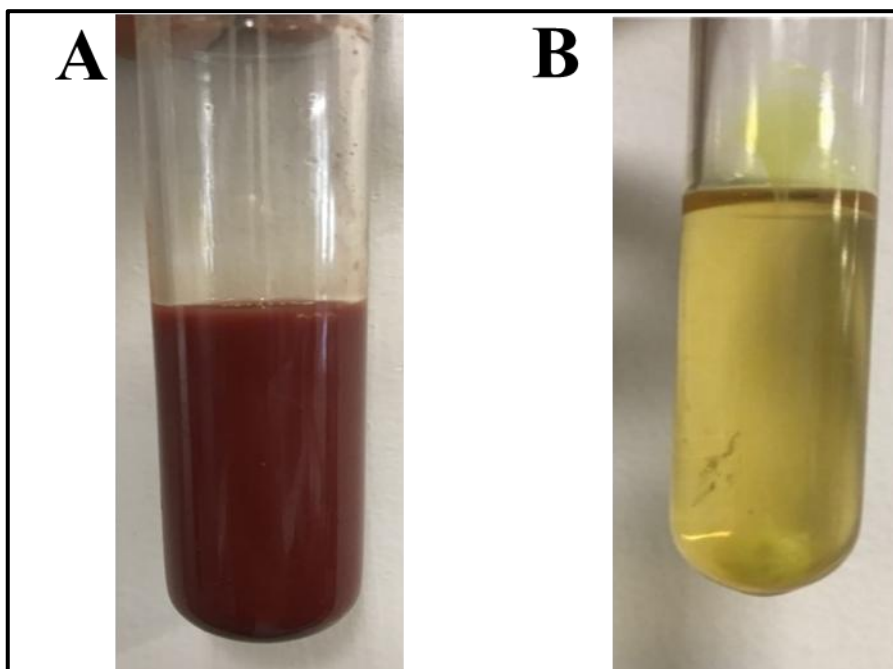


Figure 22 Cesium lead iodide perovskites solution (A) before centrifugation; and (B) after centrifugation.

a. Effect of CTAB-oleate addition

The preparation of CsPbI₃ occurred in the absence and presence of CTAB. In fact, when adding CTAB alone (solution D), the initial color of the solution was yellowish, meaning that CTAB alone does not induce the formation of perovskites. Thus, for solution A, B, and C the solution color was red orange, assuming the formation of CsPbI₃, before centrifugation (See Figure 23A). Remarkably, after centrifugation, the red color was only persisting for solution C, containing 2 mL of CTAB-oleate (added in portions) and 0.4 mL of Cs-oleate (See Figure 23B). In fact, CTAB has a dual function as a capping agent and doping of crystal. CTAB salt is dissociated into bromide ions and organic cation. With the first addition, either bromide ions are incorporated into the crystal, or the cation is replacing cesium atom. As for the second addition, CTAB acts as a capping agent to stabilize the crystal.

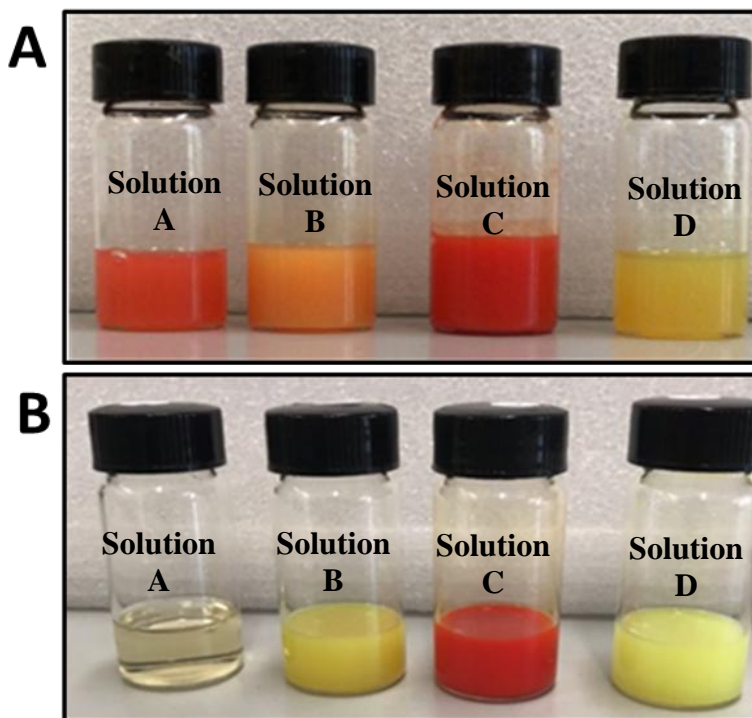


Figure 23 Color solution of cesium lead halide perovskites in the absence and presence of CTAB (A) before centrifugation; and (B) after centrifugation.

The formation of lead iodide perovskites was initially verified through X-Ray diffraction technique. As shown in Figure 24, only solution C showed three peaks at different angles. These results verify the crystal growth of CsPbI₃ perovskites in the presence of CTAB. Moreover, according to Murphy et al. [119] the main characteristic peaks of PbI₂ precursor appeared at diffraction angles of 2 θ equals to 25.96°, 34.32°, and 39.56°. These peaks were completely absent in our diffractogram confirming the absence of free PbI₂ in the solution and thus, it's incorporation into the perovskites.

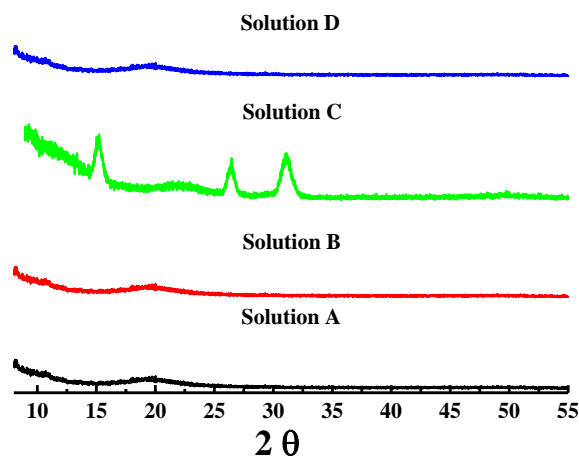


Figure 24 X-Ray Diffractogram pattern of CsPbI₃ prepared in the absence and presence of CTAB

In fact, lead iodide perovskites have 2 forms: α -CsPbI₃ and δ - CsPbI₃. However, α -CsPbI₃ is not stable and degrades rapidly to a non-perovskite yellow phase δ -CsPbI₃, when exposed to ambient air. Hence, the XRD diffractogram of α -CsPbI₃ shows peaks at 2 θ equals to 15.02° (100), 23.5° (110), and at 29.98° (200). Furthermore, δ -CsPbI₃ shows peaks at 2 θ equals to 12.9° (012), 22.5° (021), and 27.5° (122) [120]. As shown in the X-Ray diffractogram, the prepared CsPbI₃ in solution C exhibits 3 distinctive peaks at 2 θ equal to 15.1°, 23.5° and 29.07°. These peaks reveal the presence of stable

α -CsPbI₃. Hence, the amorphous structure of solution A, B, and D, proves the absence of lead iodide perovskites and therefore demonstrates the efficiency of CTAB as a surfactant, where it induces on the first hand the enhancement of crystals formation and on the second hand it inhibits their decomposition to δ -CsPbI₃.

Additionally, the successful production of perovskites was verified through the fluorescence emission spectral analysis. For this purpose, the emission spectrum for both A and C solutions, were measured at $\lambda_{\text{ex}}=500$ nm in the emission range between 550 nm and 800 nm. According to Protesescu et al. lead iodide perovskites possess an emission peak between 625-700 nm based on the obtained size [121]. As shown in Figure 25A, a clear emission peak was obtained for solution C; at $\sim \lambda_{\text{em}}= 630$ nm; thus, the same peak was totally absence for solution A. These results verify the role of CTAB as a capping agent by enhancing the formation of stable lead iodide perovskites. Likewise, no peak was observed at 780 nm which corresponds for free PbI₂, displaying the formation of stable CsPbI₃ perovskites [122]. Besides, according to Eze et al., the absorption spectrum of PbI₂ precursor shows a peak around 500 nm [123]. However, the absorption of lead iodide perovskites appears at ~ 568 nm (See Figure 25B). Thus, the identification of absorption ~ 568 nm makes it easier for establishing the formation of the perovskites in the solution. These results are in accordance with Kumar et al., where CsPbI₃ showed an absorbance edge above 500 nm [124].

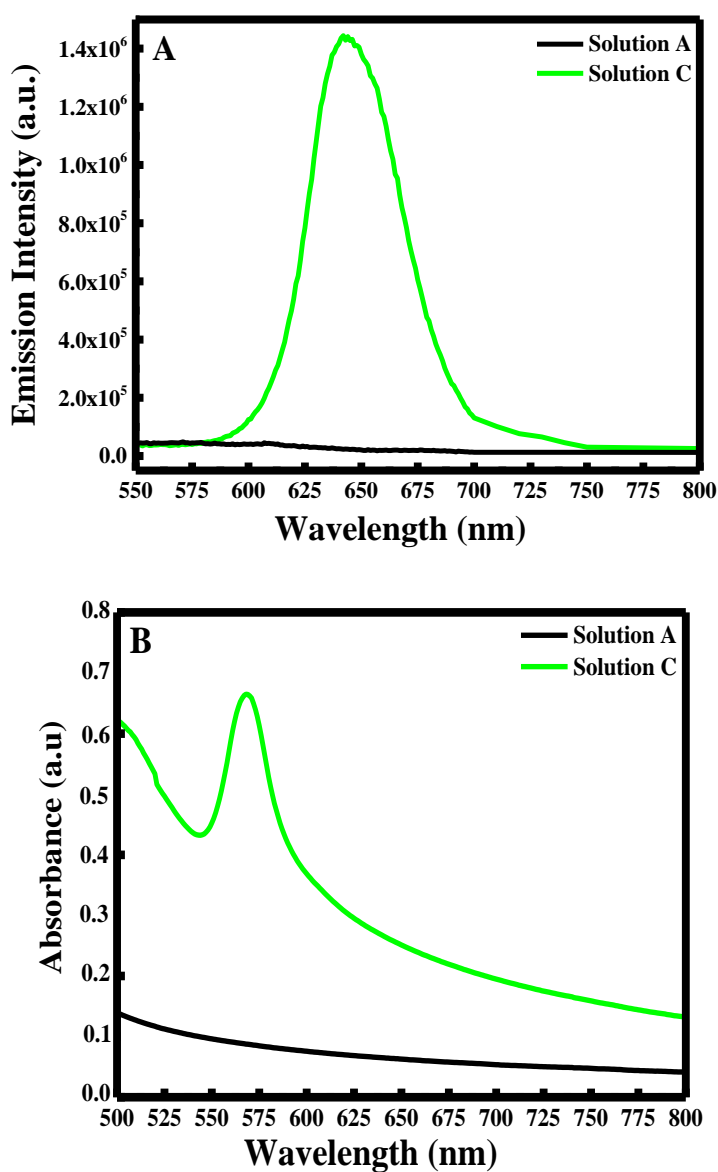


Figure 25 (A) Fluorescence emission spectra of CsPbI₃ prepared in the absence or presence of CTAB; (B) UV-Visible spectra of CsPbI₃ prepared in the absence and presence of CTAB.

Furthermore, SEM analysis was conducted in order to identify the shape of the formed α -CsPbI₃ perovskites NPs. As shown in Figure 26, the addition of CTAB encourages the formation of small, fine and uniform NPs. This was confirmed by Aleksanyan et al, where the SEM images of CsPbI₃ show uniform NPs having a near-spherical shape [125]. In fact, the formation of small particles proves the stabilization of

the black α -CsPbI₃ phase. Hence, the obtained α -CsPbI₃ NPs were highly stabilized at ambient temperature due to the presence of CTAB molecules. Indeed, according to Miyasaka et al., this is due to the presence of CTAB ions, doping therefore the perovskite and limiting its crystal growth and thus maintaining its cubic phase [126].

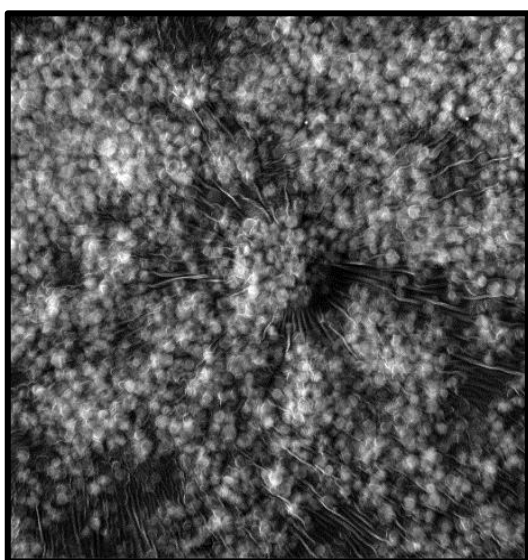


Figure 26 SEM image of CsPbI₃ prepared in the presence of CTAB.

Finally, thermo-gravimetric analysis was performed to assess the stability of the prepared perovskites. Based on the results depicted in Figure 27, CsPbI₂ perovskites lose around 5% of their mass below 100°C. Hence, this mass loss is initially related to the presence of hexane. Thus, a high mass loss around 70% was observed between 100°C – 200°C. Therefore, according to Boote et al., lead halide perovskites lose most of their masses in this temperature range due to the presence of oleylamine and oleic acid ligands [88].

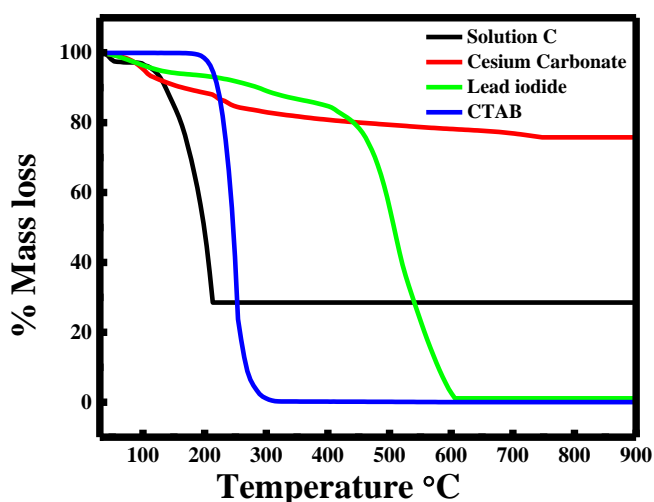


Figure 27 TGA analysis of CsPbI₃ prepared in the presence of CTAB; cesium carbonate; lead iodide; and CTAB.

b. Effect of Silica nanoparticles

On a second level, the effect of silica nanoparticles was also investigated. Similar to the results obtained when using CTAB, the formation of lead halide perovskites was only occurred in solution C, containing 2 mL of SiO₂-oleate (added in portions) and 0.4 mL of cesium oleate. This was identified visually, whereby after centrifugation the solution color remains red, verifying the formation of lead halide perovskites. The formation of cesium lead halide perovskites was initially confirmed by X-Ray diffraction technique. As shown in Figure 28, the diffraction peaks were obtained at 2θ equal to 12.1°, 23.7° and 27.9°. These diffraction peaks were similar to the peaks obtained when having δ-CsPbI₃. Hence, SiO₂ NPs encourage the formation of CsPbI₃ but with limited time stability.

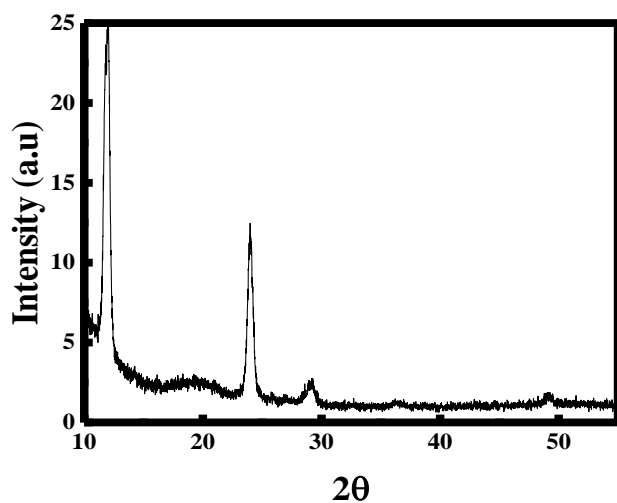


Figure 28 X-Ray diffractogram pattern of CsPbI₃ prepared in the presence of SiO₂ NPs

The formation of δ -CsPbI₃ was proved by measuring the UV-Visible spectrum of the prepared solution. As proved earlier, the identification of absorption peak 625-700 nm makes it easier for establishing the formation of the alpha perovskites in the solution. However, it is obvious from Figure 29A; an absorption peak appeared at ~450 nm. According to Cho et al., the absorption wavelength of gamma lead halide perovskites is obtained around 400 nm [127]. This proves that silica nanoparticles are involved only in the production of cesium lead halide perovskites without inducing their stability. Hence, when exciting at 325 nm, the emission wavelength of the fluorescence emission peak was obtained around ~525 nm, verifying the formation of yellow δ -CsPbI₃ (See Figure 29B).

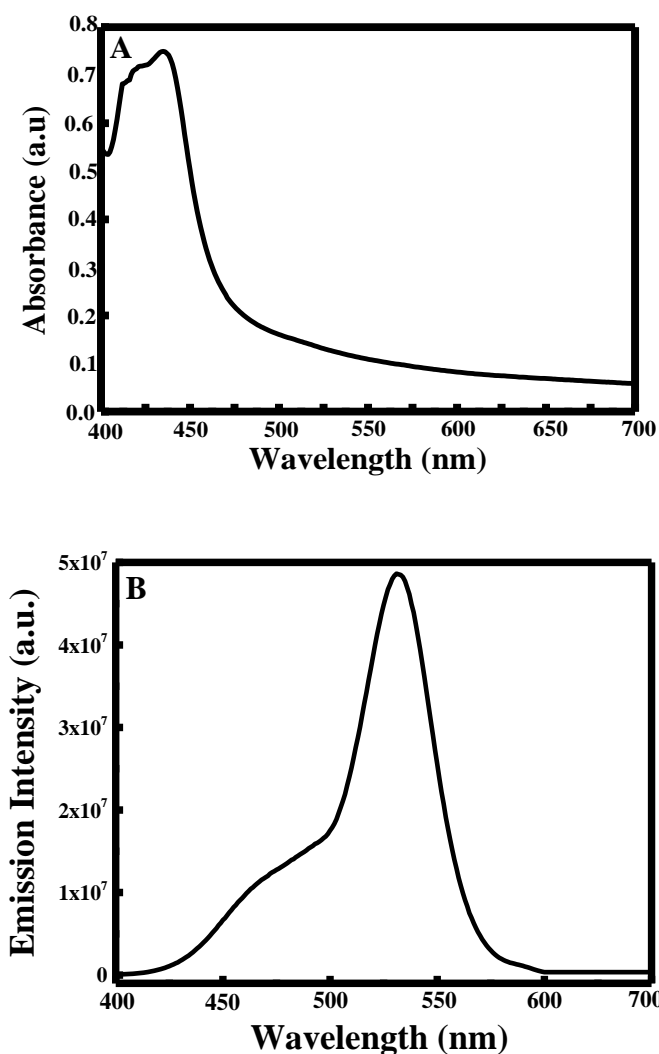


Figure 29 (A) UV-Visible spectra of CsPbI₃ prepared in the presence of SiO₂ NPs; (B) Fluorescence emission spectra of CsPbI₃ prepared in the presence of SiO₂ NPs

Furthermore, the difference between δ -CsPbI₃ and α -CsPbI₃ was easily verified through SEM analysis, where δ -CsPbI₃ were found to be in the size range between 100-120 nm (See Figure 30A), compared to the α -CsPbI₃ obtained in the presence of CTAB.

Finally, thermo-gravimetric analysis was performed, and the results are shown in Figure 30B. Similar to the results obtained when using CTAB, δ -CsPbI₂ perovskites lose around 5% of their mass below 100°C. Thus, in the presence of SiO₂ NPs a mass

loss around 100% was observed between 100°C – 200°C, where in the presence of CTAB only 70% mass loss was occurred. These results confirm the role of CTAB in the synthesis of stable α -CsPbI₃.

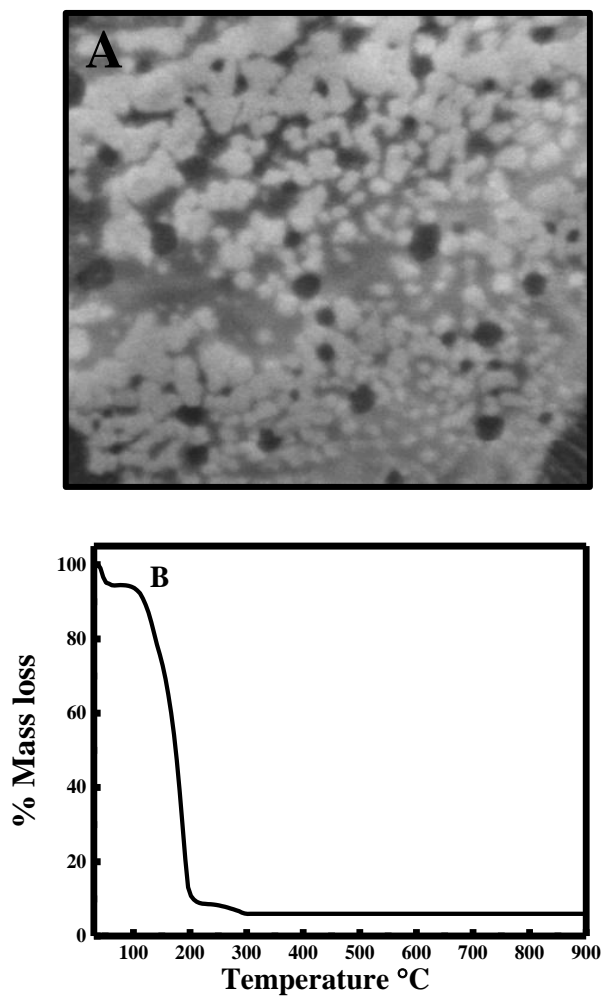


Figure 30 (A) SEM image of CsPbI₃ prepared in the presence of SiO₂ NPs; and (B) TGA analysis of CsPbI₃ prepared in the presence of SiO₂ NPs.

2. Time-dependent stability CsPbI₃ in the presence of CTAB

Lead iodide perovskites are well known to have a lack of time stability, for this reason the enhancement of their stability was found to be a great interest. The effectiveness of CTAB as capping agent was established by monitoring the color of the

solution through time for consecutive days. Interestingly, after 4 days the color of the solution containing SiO₂ NPs turned to pale brown, identifying the decomposition of α -CsPbI₃ into δ -CsPbI₃. Thus, the color of the solution containing CTAB remains almost reddish, proving the presence of only α -CsPbI₃ (See Figure 31). Therefore, CTAB enhances dramatically the stability of CsPbI₃ perovskites by preserving their crystal structure as α -CsPbI₃.

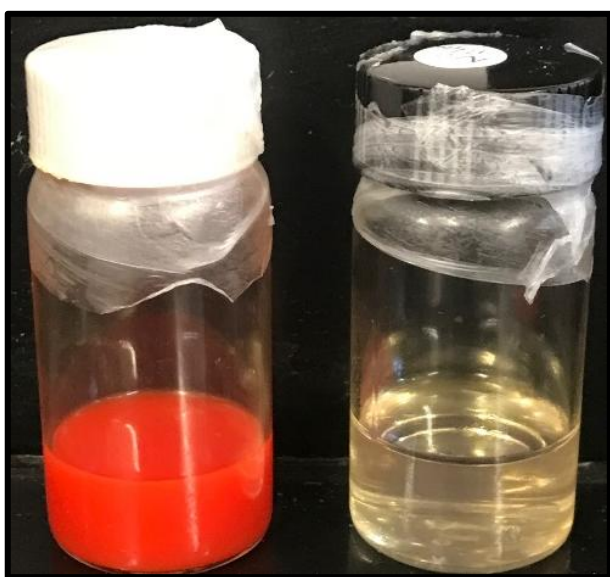


Figure 31 Solution color of CsPbI₃ after 4 consecutive days in the presence of CTAB (left side) and in the presence of SiO₂ NPs (right side).

Furthermore, the time stability of the prepared CsPbI₃ in the presence of CTAB was detected by measuring the fluorescence emission intensity within time. For this purpose, the photoluminescence stability of CsPbI₃ perovskites was studied during 4 consecutive days. As shown in Figure 32A, the formed CsPbI₃ in the presence of CTAB shows only a minimal decrease in the emission intensity without any shift in the maximum wavelength, confirming thereby the high stability of the α -CsPbI₃ phase due to the presence of CTAB.

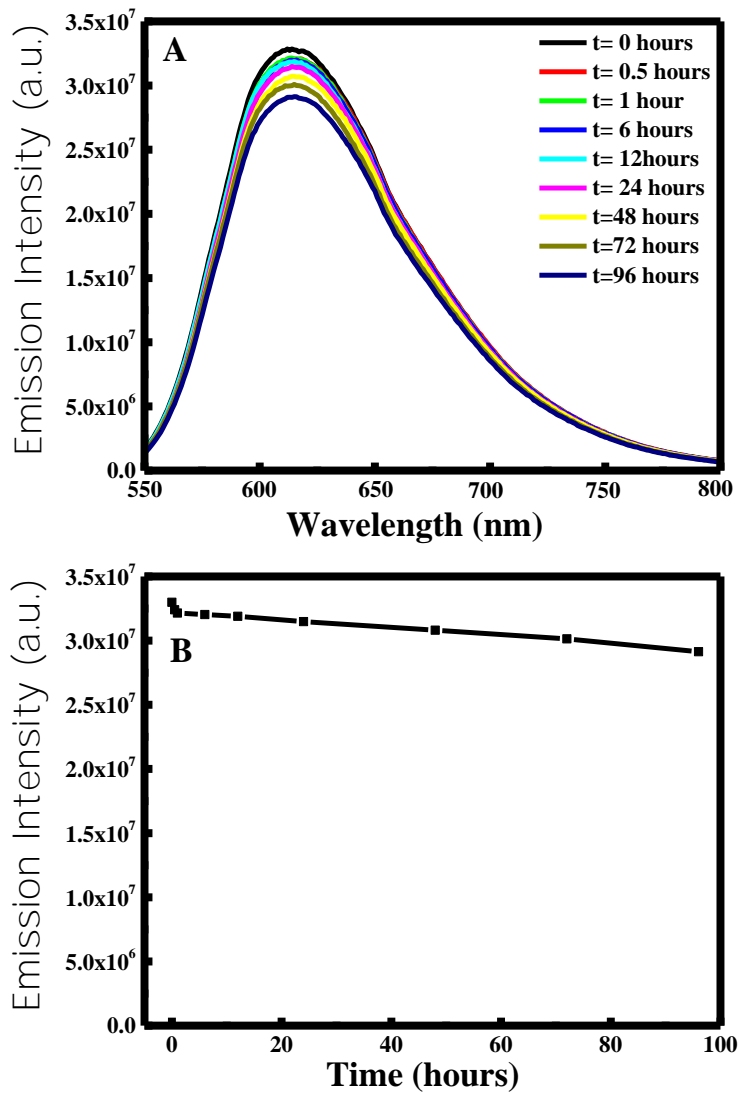


Figure 32 (A) Variation of the fluorescence emission intensity of α -CsPbI₃ in the presence of CTAB within time; (B) Maximum emission intensity vs time for α -CsPbI₃ solution in the presence of CTAB

Moreover, the PL intensity decay curve is depicted in Figure 32B by plotting the maximum emission intensity at 630 nm vs time. Henceforth, according to Ji et al, the PL intensity of CsPbI₃ NPs decreased to 35% of its initial value after 22 min of their formation [128]. Hence, in the presence of CTAB, the PL intensity of CsPbI₃ decreases by only 11.41% of its initial value after 4 days. This difference in the stability of α -

CsPbI₃ might be due to the presence of CTAB inducing the formation of smaller grains, which are responsible of the stabilization of α -CsPbI₃ phase at room temperature.

Finally, the absence of the wavelength shift was also confirmed calorimetrically, by observing the solution color within time. Remarkably, the solution color remains reddish, confirming the presence of α -CsPbI₃ (See Figure 33).

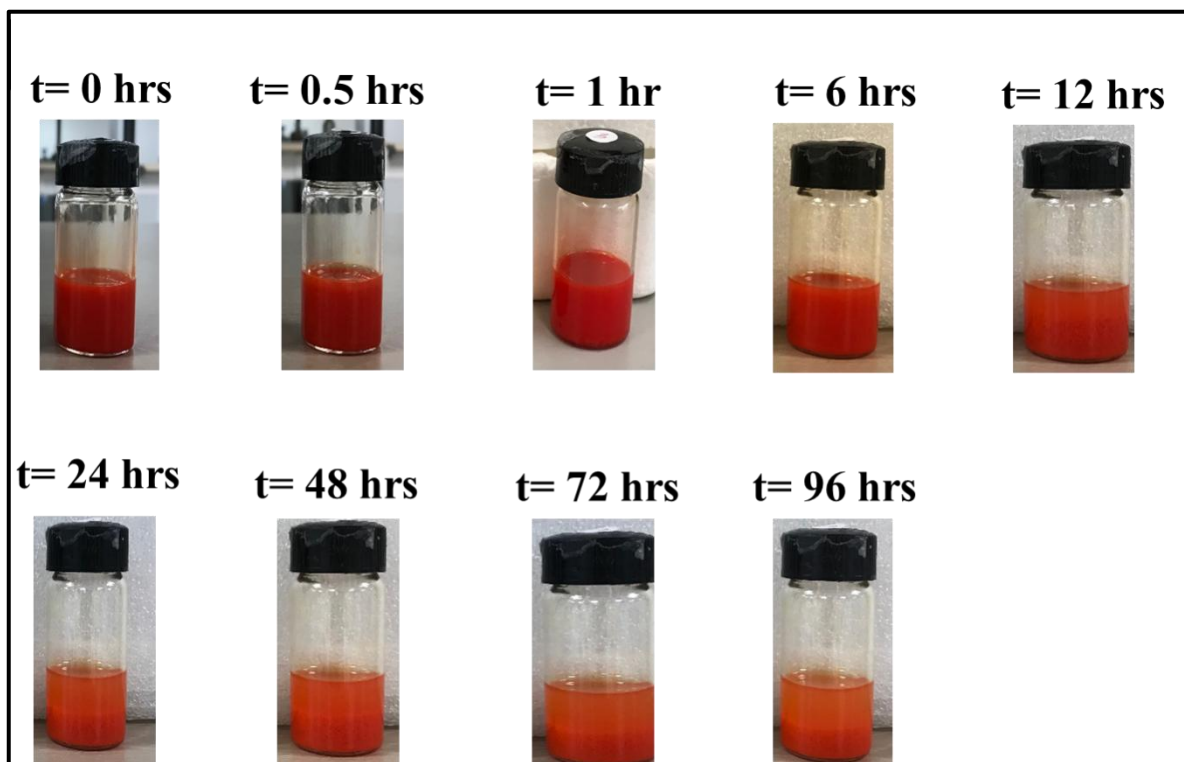


Figure 33 Color change of α -CsPbI₃ in the presence of CTAB solution within time.

3. PLQY measurements in the presence/absence of CTAB and SiO₂ NPs

The reference used to determine the Photoluminescence quantum yield was Rhodamine 6G having $\eta = 0.95$ and an emission range of 500-700 nm. The synthesized CsPbI₃ were analyzed by Fluorometry technique in the presence of either CTAB or Si NPs.

Interestingly, the PLQY % of CsPbI₃ was enhanced to reach ~99% when CTAB was added to the solution compared with ~70% when SiO₂ NPs were added. This increase (~1.2 fold) is due to the enhancement of the stability of the synthesized perovskites upon doping it with CTAB having methylammonium groups. Different PLQY values found in the literature were summarized in Table 1.

Perovskites prepared	PLQY (%)	References
AET-CsPbI ₃	51	[129]
CsPbI ₃ QDs with variation of the Zn/Pb ratio	93	[130]
CsPbI ₃ QDs/PVDF nanofibers	11	[131]
α -CsPbI ₃ with Mn ²⁺ Doping	90	[128]
CsPbI ₃ /TOPO	47.2	[132]
CTAB doped CsPbI ₃	99	Our work

Table 5 Different PLQY (%) values found in the literature for CsPbI₃ perovskites.

D. Conclusion

In conclusion, CsPbI₃ NCs have become promising materials in red-emitting due to their exceptional optical properties; however, their poor stability has severely limited their development. It was verified that CTAB was a better stabilizing agent than Si NPs which decomposes totally after 4 days. Moreover, the presence of CTAB is critical in terms of stabilizing the α -CsPbI₃ phase, boosting the PLQY % and increasing the photoluminescence stability. Primarily, the presence of CTAB maintained the α -CsPbI₃ phase and prevents its transformation into other phases. Furthermore, the addition of CTAB boosted the PLQY to 99%. Finally, the PL intensity peak was enhanced and degraded by only 11.41% with CTAB doping.

CHAPTER VII

CONCLUSION

In conclusion, CsPbBr₃ and CsPbI₃ perovskites were synthesized through a simple method by hot-injection process. Upon optimization, it was found that the most stable and smallest CsPbBr₃ NPs were formed when 0.0226 g of cesium oleate was added in the presence of 0.15 g of PbBr₂ for 40 minutes. The formed NPs maintained their 3D structure due to the direct quenching of the solution.

Furthermore, it was verified that the addition of CTAB is crucial in terms of the enhancement of the photoluminescence stability where it decreases by only ~15% within 4 days. Henceforth, the presence of CTAB stabilizes the incorporation of PbBr₂ inside the perovskites, where the formed CsPbBr₃ loses only around ~10% of their total mass. Moreover, the addition of CTAB boosted the PLQY to reach 75%, compared with 16% in the absence of CTAB.

Interestingly, it was verified that CPB was a better stabilizing agent than CTAB due to the attachment of cetylpyridinium and bromide ions to the surface defects of the CsPbBr₃ crystals. This resulted in the formation of a multitude of small and uniform CsPbBr₃ NPs. Henceforth, the presence of CPB increases the thermal stability of CsPbBr₃ due to the presence of pyridinium groups that promote the incorporation of PbBr₂ inside the perovskites. Moreover, the addition of CPB boosted the PLQY to 90%. It was verified that CPB acts as a capping agent in preserving the crystal structure of CsPbBr₃ and protecting it from any interactions with the surrounding. Furthermore, CPB prevents any anion exchange between bromide and iodide ions when low concentrations of PbI₂ are added.

On the other hand, CsPbI₃ NPs have become promising materials in red-emitting applications. However, they are unstable and thus at ambient temperature, α -CsPbI₃ is directly decomposed into the non-perovskite yellow δ -CsPbI₃ phase. It was verified that when CTAB was used, α -CsPbI₃ phase was maintained. However, this phase decomposes totally after 4 days with the addition of Si NPs. Thus, CTAB was a better stabilizing agent than Si NPs in terms of stabilizing the α -CsPbI₃ phase and preventing its transformation into other phases. Moreover, the presence of CTAB is critical in boosting the PLQY to 99%. Henceforth, the PL intensity peak was enhanced where it degraded by only 11.41% with CTAB doping.

Other potentially fruitful areas for further research that emerged from our study are its possible applications. The synthesized perovskites could be used in the sensing of glucose and H₂O₂. Henceforth, the effect of anion exchange on the stability of perovskites could be elaborated by mixing both equal concentrations of bromide and iodide ions during the synthesis of perovskites. Moreover, CPB could be used as a capping agent to enhance the stability of CsPbI₃ perovskites.

REFERENCES

- [1] Z. Cheng and J. Lin, "Layered organic-inorganic hybrid perovskites: Structure, optical properties, film preparation, patterning and templating engineering," *CrystEngComm*, vol. 12, no. 10, pp. 2646–2662, 2010, doi: 10.1039/c001929a.
- [2] N. F. Atta, A. Galal, and E. H. El-Ads, "Perovskite Nanomaterials – Synthesis, Characterization, and Applications," in *Perovskite Materials - Synthesis, Characterisation, Properties, and Applications*, 2016, p. 46.
- [3] M. A. Green, A. Ho-Baillie, and H. J. Snaith, "The emergence of perovskite solar cells," *Nat. Photonics*, vol. 8, no. 7, pp. 506–514, 2014, doi: 10.1038/nphoton.2014.134.
- [4] E. A. R. Assirey, "Perovskite synthesis, properties and their related biochemical and industrial application," *Saudi Pharm. J.*, vol. 27, no. 6, pp. 817–829, 2019, doi: 10.1016/j.jsps.2019.05.003.
- [5] G. Niu, X. Guo, and L. Wang, "Review of recent progress in chemical stability of perovskite solar cells," *J. Mater. Chem. A*, vol. 3, no. 17, pp. 8970–8980, 2015, doi: 10.1039/c4ta04994b.
- [6] H. Rétot, A. Bessière, A. Kahn-Harari, and B. Viana, "Synthesis and optical characterization of SrHfO₃:Ce and SrZrO₃:Ce nanoparticles," *Opt. Mater. (Amst.)*, vol. 30, no. 7, pp. 1109–1114, 2008, doi: 10.1016/j.optmat.2007.05.032.
- [7] L. Eric Cross, "Relaxor ferroelectrics," *Ferroelectrics*, vol. 76, no. 1, pp. 241–267, 1987, doi: 10.1080/00150198708016945.
- [8] R. J. Cava, "Feature 5," *J. Am. Ceram. Soc.*, vol. 83, no. 1, pp. 5–28, 2000.
- [9] X. Wang, J. Zhou, J. Song, J. Liu, N. Xu, and Z. L. Wang, "Piezoelectric field effect transistor and nanoforce sensor based on a single ZnO nanowire," *Nano Lett.*, vol. 6, no. 12, pp. 2768–2772, 2006, doi: 10.1021/nl061802g.
- [10] J. Wang, S. Q. Shi, L. Q. Chen, Y. Li, and T. Y. Zhang, "Phase-field simulations of ferroelectric/ferroelastic polarization switching," *Acta Mater.*, vol. 52, no. 3, pp. 749–764, 2004, doi: 10.1016/j.actamat.2003.10.011.
- [11] Y. Nishihata, J. Mizuki, H. Tanaka, M. Uenishi, and M. Kimura, "Self-regeneration of palladium-perovskite catalysts in modern automobiles," *J. Phys. Chem. Solids*, vol. 66, no. 2–4, pp. 274–282, 2005, doi: 10.1016/j.jpcs.2004.06.090.
- [12] J. Taylor, K. Zhang, and D. Wang, *Industrial and nonfood applications*. AACCI, 2018.
- [13] A. Ottochian, G. Dezanneau, C. Gilles, P. Raiteri, C. Knight, and J. D. Gale, "Influence of isotropic and biaxial strain on proton conduction in Y-doped BaZrO₃: A reactive molecular dynamics study," *J. Mater. Chem. A*, vol. 2, no. 9, pp. 3127–3133, 2014, doi: 10.1039/c3ta12800h.
- [14] Z. Zhang, S. Gu, Y. Ding, F. Zhang, and J. Jin, "Determination of hydrogen peroxide and glucose using a novel sensor platform based on Co_{0.4}Fe_{0.6}LaO₃ nanoparticles," *Microchim. Acta*, vol. 180, no. 11–12, pp. 1043–1049, 2013, doi: 10.1007/s00604-013-1012-9.
- [15] S. Thirumalairajan, K. Giriya, N. Y. Hebalkar, D. Mangalaraj, C. Viswanathan, and N. Ponpandian, "Shape evolution of perovskite LaFeO₃ nanostructures: A systematic investigation of growth mechanism, properties and morphology dependent photocatalytic activities," *RSC Adv.*, vol. 3, no. 20, pp. 7549–7561, 2013, doi: 10.1039/c3ra00006k.

- [16] F. Wang, D. Chen, and Z. Shao, "Sm_{0.5}Sr_{0.5}CoO_{3-δ}-infiltrated cathodes for solid oxide fuel cells with improved oxygen reduction activity and stability," *J. Power Sources*, vol. 216, pp. 208–215, 2012, doi: 10.1016/j.jpowsour.2012.05.068.
- [17] S. Nieto, R. Polanco, and R. Roque-malherbe, "Absorption Kinetics of Hydrogen In Nanocrystals of BaCe_{0.95}Yb_{0.05}O_{3-δ} Proton-Conducting Perovskite," *Phys. Chem. C.*, vol. 111, pp. 2809–2818, 2007.
- [18] P. M. Mankiewich, J. H. Scofield, W. J. Skocpol, R. E. Howard, A. H. Dayem, and E. Good, "Reproducible technique for fabrication of thin films of high transition temperature superconductors," *Appl. Phys. Lett.*, vol. 51, no. 21, pp. 1753–1755, 1987, doi: 10.1063/1.98513.
- [19] Y. B. Pottathara and S. Thomas, "Synthesis and Processing of Emerging Two-Dimensional Nanomaterials," *ScienceDirect*, 2019.
- [20] T. Nakamura, M. Misono, and Y. Yoneda, "Reduction-oxidation and catalytic properties of La_{1-x}Sr_xCoO₃," *J. Catal.*, vol. 83, no. 1, pp. 151–159, 1983, doi: 10.1016/0021-9517(83)90038-6.
- [21] S. Esposito, "'Traditional' sol-gel chemistry as a powerful tool for the preparation of supported metal and metal oxide catalysts," *Materials (Basel)*, vol. 12, no. 4, pp. 1–25, 2019, doi: 10.3390/ma12040668.
- [22] E. Kemnitz and J. Noack, "The non-aqueous fluorolytic sol-gel synthesis of nanoscaled metal fluorides," *R. Soc. Chem.*, vol. 44, pp. 19411–19431, 2015, doi: 10.1039/c5dt00914f.
- [23] A. D. Lozano-Gorrin, "Structural Characterization of New Perovskites," in *Intech*, 2012, pp. 107–204.
- [24] M. Lusi, "Engineering Crystal Properties through Solid Solutions," *Am. Chem. Soc.*, vol. 18, pp. 3704–3712, 2018, doi: 10.1021/acs.cgd.7b01643.
- [25] K. W. Tan *et al.*, "Evolution and Performance of Solar Cells," no. 5, pp. 4730–4739, 2014.
- [26] K. Korshunova, L. Winterfeld, W. J. D. Beenken, and E. Runge, "Thermodynamic stability of mixed Pb:Sn methyl-ammonium halide perovskites," *basic solid state Phys.*, vol. 1915, no. 10, pp. 1907–1915, 2016, doi: 10.1002/pssb.201600136.
- [27] T. Sato, S. Takagi, S. Deledda, B. C. Hauback, and S. Orimo, "Extending the applicability of the Goldschmidt tolerance factor to arbitrary ionic compounds," *Nat. Publ. Gr.*, no. January, pp. 1–10, 2016, doi: 10.1038/srep23592.
- [28] P. S. B. Grocholski, "Natural and engineered 732 10," *Science (80-.)*, vol. 358, no. 6364, pp. 732–734, 2017.
- [29] F. Wetenschappen, D. Fysica, A. D. U. Antwerpen, and R. P. Sena, "Structure characterization of triple perovskites and related systems by transmission electron microscopy Structuurbepaling van triple perovskieten en gerelateerde systemen aan de hand van transmissie elektronenmicroscopie," 2017.
- [30] B. Conings, L. Baeten, C. De Dobbelaere, J. D. Haen, and J. Manca, "Perovskite-Based Hybrid Solar Cells Exceeding 10 % Efficiency with High Reproducibility Using a Thin Film Sandwich Approach," *Adv. Mater.*, vol. 26, pp. 2041–2046, 2014, doi: 10.1002/adma.201304803.
- [31] I. T, *Perovskite Oxide for Solid Oxide Fuel Cells*. .
- [32] Y. Zhou, J. Chen, O. M. Bakr, and H. Sun, "Metal-Doped Lead Halide Perovskites : Synthesis , Properties , and Optoelectronic Applications," *Chem.*

- Mater.*, vol. 30, pp. 6589–6613, 2018, doi: 10.1021/acs.chemmater.8b02989.
- [33] B. A. Rosales, L. Wei, and J. Vela, “Synthesis and mixing of complex halide perovskites by solvent-free solid-state methods,” *J. Solid State Chem.*, vol. 271, no. September 2018, pp. 206–215, 2019, doi: 10.1016/j.jssc.2018.12.054.
- [34] A. R. B. M. Yusoff and M. K. Nazeeruddin, “Organohalide Lead Perovskites for Photovoltaic Applications,” *J. Phys. Chem. Lett.*, vol. 7, no. 5, pp. 851–866, 2016, doi: 10.1021/acs.jpcclett.5b02893.
- [35] J. K. Kim, S. S. Kim, and W. J. Kim, “Sol-gel synthesis and properties of multiferroic BiFeO₃,” *Mater. Lett.*, vol. 59, no. 29–30, pp. 4006–4009, 2005, doi: 10.1016/j.matlet.2005.07.050.
- [36] Z. Xiao *et al.*, “Single-crystal nanofibers of Zr-doped new structured PbTiO₃: Hydrothermal synthesis, characterization and phase transformation,” *J. Mater. Chem.*, vol. 21, no. 11, pp. 3562–3564, 2011, doi: 10.1039/c0jm04212a.
- [37] N. H. Yusoff, R. A. M. Osman, M. S. Idris, K. N. D. K. Muhsen, and N. I. M. Nor, “Dielectric and structural analysis of hexagonal and tetragonal phase BaTiO₃,” *AIP Conf. Proc.*, vol. 2203, no. January, pp. 1–8, 2020, doi: 10.1063/1.5142130.
- [38] Q. Zhang, R. Su, X. Liu, J. Xing, T. C. Sum, and Q. Xiong, “High-Quality Whispering-Gallery-Mode Lasing from Cesium Lead Halide Perovskite Nanoplatelets,” *Adv. Funct. Mater.*, vol. 26, no. 34, pp. 6238–6245, 2016, doi: 10.1002/adfm.201601690.
- [39] W. L. Hong *et al.*, “Efficient Low-Temperature Solution-Processed Lead-Free Perovskite Infrared Light-Emitting Diodes,” *Adv. Mater.*, vol. 28, no. 36, pp. 8029–8036, 2016, doi: 10.1002/adma.201601024.
- [40] K. Wu, G. Liang, Q. Shang, Y. Ren, D. Kong, and T. Lian, “Ultrafast Interfacial Electron and Hole Transfer from CsPbBr₃ Perovskite Quantum Dots,” *J. Am. Ceram. Soc.*, vol. 137, pp. 12792–12795, 2015, doi: 10.1021/jacs.5b08520.
- [41] L. Protesescu *et al.*, “Nanocrystals of Cesium Lead Halide Perovskites (CsPbX₃, X = Cl, Br, and I): Novel Optoelectronic Materials Showing Bright Emission with Wide Color Gamut,” *Nano Lett.*, vol. 15, pp. 3692–3696, 2015, doi: 10.1021/nl5048779.
- [42] U. Resch-Genger and K. Rurack, “Determination of the photoluminescence quantum yield of dilute dye solutions (IUPAC Technical Report),” *Pure Appl. Chem.*, vol. 85, no. 10, pp. 2005–2026, 2013, doi: 10.1351/PAC-REP-12-03-03.
- [43] K. Moorjani *et al.*, *High-temperature superconductivity*, vol. 11, no. 1–2. 1990.
- [44] M. Morita, H. Teshima, and H. Hirano, “Development of oxide superconductors - High-Tc bulk superconductor, QMG, and its magnetic applications - High-Tc b,” 2006.
- [45] T. Kleckers, “A1.1 - Electrical Strain Gauges, Piezoelectric Sensors or Fiber Bragg Sensors for Force Measurement: Prospects and Potentials,” in *Electrical Strain Gauges, Piezoelectric Sensors or Fiber Bragg Sensors for Force Measurement: Prospects and Potentials*, 2020, pp. 23–27, doi: 10.5162/sensor2013/a1.1.
- [46] N. A. Spaldin, S. Cheong, and R. Ramesh, “Multiferroics : Past , present , and future feature,” *Phys. Today*, vol. 38, no. 2010, pp. 38–43, 2016, doi: 10.1063/1.3502547.
- [47] F. Wang, C. Li, T. Zou, Y. Liu, and Y. Sun, “Electrically driven magnetic relaxation in Electrically driven magnetic relaxation in multiferroic LuFe₂O₄,”

- 2010, doi: 10.1088/0953-8984/22/49/496001.
- [48] A. Ghosh, D. P. Trujillo, H. Choi, and S. M. Nakhmanson, “Electronic and Magnetic Properties of Lanthanum and Strontium Doped Bismuth Ferrite : A First-Principles Study,” *Sci. Rep.*, no. October 2018, pp. 1–10, 2019, doi: 10.1038/s41598-018-37339-3.
- [49] C. Psaroudaki and X. Zotos, “Magnetic and magnetothermal properties and the magnetic phase diagram of high purity single crystalline terbium along the easy magnetization direction,” *J. Phys.*, p. 7, 2014, doi: 10.1088/0953-8984/26/6/066001.
- [50] B. Raveau, A. Maignan, C. Martin, and M. Hervieu, “Colossal Magnetoresistance Manganite Perovskites: Relations between Crystal Chemistry and Properties,” *Chem. Mater.*, vol. 10, no. 10, pp. 2641–2652, 1998, doi: 10.1021/cm9801791.
- [51] Q. Shen, S. Dong, S. Li, G. Yang, and X. Pan, “A review on the catalytic decomposition of NO_x by perovskite-type oxides,” *Catalysts*, vol. 11, no. 5, 2021, doi: 10.3390/catal11050622.
- [52] M. Sharma, M. Pathak, and P. N. Kapoor, “The sol-gel method: Pathway to ultrapure and homogeneous mixed metal oxide nanoparticles,” *Asian J. Chem.*, vol. 30, no. 7, pp. 1405–1412, 2018, doi: 10.14233/ajchem.2018.20845.
- [53] D. Dijkkamp *et al.*, “Preparation of Y-Ba-Cu oxide superconductor thin films using pulsed laser evaporation from high T_c bulk material,” *Appl. Phys. Lett.*, vol. 51, no. 8, pp. 619–621, 1987, doi: 10.1063/1.98366.
- [54] X. D. Wu *et al.*, “Low-temperature preparation of high T_c superconducting thin films,” *Appl. Phys. Lett.*, vol. 52, no. 9, pp. 754–756, 1988, doi: 10.1063/1.99337.
- [55] H. Adachi, T. Mitsuyu, O. Yamazaki, and K. Wasa, “Ferroelectric $(\text{Pb,L a})(\text{Zr,T i})\text{O}_3$ epitaxial thin films on sapphire grown by rf-planar magnetron sputtering,” *J. Appl. Phys.*, vol. 60, no. 2, pp. 736–741, 1986, doi: 10.1063/1.337423.
- [56] Z. Han *et al.*, “Single-target sputter deposition, post-processing and electron spectroscopy of perovskite superconductor thin films,” in *Single-target sputter deposition, post-processing and electron spectroscopy of perovskite superconductor thin films*, 2008, vol. 66, pp. 66–70, doi: 10.1063/1.37082.
- [57] P. Berberich, J. Tate, W. Dietsche, and H. Kinder, “Low-temperature preparation of superconducting $\text{YBa}_2\text{Cu}_3\text{O}_{7-\delta}$ films on Si, MgO, and SrTiO_3 by thermal coevaporation,” *Appl. Phys. Lett.*, vol. 53, no. 10, pp. 925–926, 1988, doi: 10.1063/1.100647.
- [58] R. Boston, K. Awaya, T. Nakayama, W. Ogasawara, and S. R. Hall, “Formation of superconducting yttrium barium copper oxide using sulphur-containing templates,” *RSC Adv.*, vol. 4, no. 51, pp. 26824–26828, 2014, doi: 10.1039/c4ra04745a.
- [59] M. Shandilya, R. Rai, and J. Singh, “Review: Hydrothermal technology for smart materials,” *Adv. Appl. Ceram.*, vol. 115, no. 6, pp. 354–376, 2016, doi: 10.1080/17436753.2016.1157131.
- [60] V. G. Kessler, G. I. Spijksma, G. A. Seisenbaeva, S. Håkansson, D. H. A. Blank, and H. J. M. Bouwmeester, “New insight in the role of modifying ligands in the sol-gel processing of metal alkoxide precursors: A possibility to approach new classes of materials,” *J. Sol-Gel Sci. Technol.*, vol. 40, no. 2–3, pp. 163–179,

- 2006, doi: 10.1007/s10971-006-9209-6.
- [61] A. Feinle, M. S. Elsaesser, and N. Hüsing, “Sol-gel synthesis of monolithic materials with hierarchical porosity,” *Chem. Soc. Rev.*, vol. 45, no. 12, pp. 3377–3399, 2016, doi: 10.1039/c5cs00710k.
- [62] R. Schmidt, J. P. Gonjal, and E. Morán, “Microwaves: Microwave-Assisted Hydrothermal Synthesis of Nanoparticles,” *CRC Concise Encycl. Nanotechnol.*, no. January 2016, pp. 588–599, 2018, doi: 10.1201/b19457-51.
- [63] T. Alammar, I. Hamm, V. Grasmik, M. Wark, and A. V. Mudring, “Microwave-Assisted Synthesis of Perovskite SrSnO₃ Nanocrystals in Ionic Liquids for Photocatalytic Applications,” *Inorg. Chem.*, vol. 56, no. 12, pp. 6920–6932, 2017, doi: 10.1021/acs.inorgchem.7b00279.
- [64] H. M. Christen and G. Eres, “Recent advances in pulsed-laser deposition of complex oxides,” *J. Phys. Condens. Matter*, vol. 20, no. 26, 2008, doi: 10.1088/0953-8984/20/26/264005.
- [65] M. Shellaiiah and K. W. Sun, “Review on Sensing Applications of Perovskite Nanomaterials,” *Chemosensors*, vol. 8, no. 3, p. 55, 2020, doi: 10.3390/chemosensors8030055.
- [66] E. H. El-Ads, A. Galal, and N. F. Atta, “Electrochemistry of glucose at gold nanoparticles modified graphite/SrPdO₃ electrode - Towards a novel non-enzymatic glucose sensor,” *J. Electroanal. Chem.*, vol. 749, pp. 42–52, 2015, doi: 10.1016/j.jelechem.2015.04.033.
- [67] S. Malkhandi, B. Yang, A. K. Manohar, A. Manivannan, G. K. S. Prakash, and S. R. Narayanan, “Electrocatalytic properties of nanocrystalline calcium-doped lanthanum cobalt oxide for bifunctional oxygen electrodes,” *J. Phys. Chem. Lett.*, vol. 3, no. 8, pp. 967–972, 2012, doi: 10.1021/jz300181a.
- [68] Q. Chen *et al.*, “Under the spotlight: The organic-inorganic hybrid halide perovskite for optoelectronic applications,” *Nano Today*, vol. 10, no. 3, pp. 355–396, 2015, doi: 10.1016/j.nantod.2015.04.009.
- [69] D. Bryant *et al.*, “Light and oxygen induced degradation limits the operational stability of methylammonium lead triiodide perovskite solar cells,” *Energy Environ. Sci.*, vol. 9, no. 5, pp. 1655–1660, 2016, doi: 10.1039/c6ee00409a.
- [70] Z. Shao and S. M. Halle, “A high-performance cathode for the next generation of solid-oxide fuel cells,” *Nature*, vol. 431, no. 7005, pp. 170–173, 2004, doi: 10.1038/nature02863.
- [71] H. Zhu *et al.*, “Lead halide perovskite nanowire lasers with low lasing thresholds and high quality factors,” *Nat. Mater.*, vol. 14, no. 6, pp. 636–642, 2015, doi: 10.1038/nmat4271.
- [72] J. Song, J. Li, X. Li, L. Xu, Y. Dong, and H. Zeng, “Quantum Dot Light-Emitting Diodes Based on Inorganic Perovskite Cesium Lead Halides (CsPbX₃),” *Adv. Mater.*, vol. 27, no. 44, pp. 7162–7167, 2015, doi: 10.1002/adma.201502567.
- [73] J. Liu *et al.*, “Two-Dimensional CH₃NH₃PbI₃ Perovskite: Synthesis and Optoelectronic Application,” *ACS Nano*, vol. 10, no. 3, pp. 3536–3542, 2016, doi: 10.1021/acsnano.5b07791.
- [74] H. Deng *et al.*, “Growth, patterning and alignment of organolead iodide perovskite nanowires for optoelectronic devices,” *Nanoscale*, vol. 7, no. 9, pp. 4163–4170, 2015, doi: 10.1039/c4nr06982j.
- [75] Y. Han *et al.*, “Degradation observations of encapsulated planar CH₃NH₃PbI₃

- perovskite solar cells at high temperatures and humidity,” *J. Mater. Chem. A*, vol. 3, no. 15, pp. 8139–8147, 2015, doi: 10.1039/c5ta00358j.
- [76] Q. Dong *et al.*, “Encapsulation of Perovskite Solar Cells for High Humidity Conditions,” *ChemSusChem*, vol. 9, no. 18, pp. 2597–2603, 2016, doi: 10.1002/cssc.201600868.
- [77] N. Aristidou *et al.*, “The Role of Oxygen in the Degradation of Methylammonium Lead Trihalide Perovskite Photoactive Layers,” *Angew. Chemie - Int. Ed.*, vol. 54, no. 28, pp. 8208–8212, 2015, doi: 10.1002/anie.201503153.
- [78] J. J. Carpay, F. H. Nieman, K. G. König, A. J. Felling, and J. G. Lammers, “Quality of dental restorations and dental treatment in Dutch schoolchildren,” *Community Dent. Health*, vol. 7, no. 1, pp. 43–51, 1990.
- [79] Y. B. Pottathara, Y. Grohens, V. Kokol, N. Kalarikkal, and S. Thomas, *Synthesis and processing of emerging two-dimensional nanomaterials*. Elsevier Inc., 2019.
- [80] M. I. Alturisa, J. Wira, Mardiyati, Herman, and R. Hidayat, “Influences of Precursor Solution Concentration and Temperature on CH₃NH₃PbI₃ Perovskite Layer Morphology and the Unconverted PbI₂ Proportion to their Perovskite Solar Cell Characteristics,” *J. Phys. Conf. Ser.*, vol. 877, no. 1, 2017, doi: 10.1088/1742-6596/877/1/012046.
- [81] S. Wiegand *et al.*, “Precursor Concentration Affects Grain Size, Crystal Orientation, and Local Performance in Mixed-Ion Lead Perovskite Solar Cells,” *ACS Appl. Energy Mater.*, vol. 1, no. 12, pp. 6801–6808, 2018, doi: 10.1021/acsaem.8b00913.
- [82] W. C. de Gruijter, “Luminescence of lead chloride and lead bromide single crystals: I. The excitation and emission spectra,” *J. Solid State Chem.*, vol. 6, no. 1, pp. 151–162, 1973, doi: 10.1016/0022-4596(73)90214-4.
- [83] E. Belarbi *et al.*, “Transformation of PbI₂, PbBr₂ and PbCl₂ salts into MAPbBr₃ perovskite by halide exchange as an effective method for recombination reduction,” *Phys. Chem. Chem. Phys.*, vol. 19, no. 17, pp. 10913–10921, 2017, doi: 10.1039/c7cp01192j.
- [84] X. Fang *et al.*, “Effect of excess PbBr₂ on photoluminescence spectra of CH₃NH₃PbBr₃ perovskite particles at room temperature,” *Appl. Phys. Lett.*, vol. 108, no. 7, pp. 1–5, 2016, doi: 10.1063/1.4942410.
- [85] J. H. Cha *et al.*, “Photoresponse of CsPbBr₃ and Cs₄PbBr₆ Perovskite Single Crystals,” *J. Phys. Chem. Lett.*, vol. 8, no. 3, pp. 565–570, 2017, doi: 10.1021/acs.jpcclett.6b02763.
- [86] Z. Shi *et al.*, “High-efficiency and air-stable perovskite quantum dots light-emitting diodes with an all-inorganic heterostructure,” *Nano Lett.*, vol. 17, no. 1, pp. 313–321, 2017, doi: 10.1021/acs.nanolett.6b04116.
- [87] F. De Matteis *et al.*, “Optical characterization of cesium lead bromide perovskites,” *Crystals*, vol. 9, no. 6, pp. 1–13, 2019, doi: 10.3390/cryst9060280.
- [88] B. W. Boote *et al.*, “Unveiling the Photo- and Thermal-Stability of Cesium Lead Halide Perovskite Nanocrystals,” *ChemPhysChem*, vol. 20, no. 20, pp. 2647–2656, 2019, doi: 10.1002/cphc.201900432.
- [89] P. Acharyya, P. Pal, P. K. Samanta, A. Sarkar, S. K. Pati, and K. Biswas, “Single pot synthesis of indirect band gap 2D CsPb₂Br₅ nanosheets from direct band gap 3D CsPbBr₃ nanocrystals and the origin of their luminescence properties,” *Nanoscale*, vol. 11, no. 9, pp. 4025–4034, 2019, doi: 10.1039/c8nr09349k.

- [90] H. J. Snaith, "Perovskites: The emergence of a new era for low-cost, high-efficiency solar cells," *J. Phys. Chem. Lett.*, vol. 4, no. 21, pp. 3623–3630, 2013, doi: 10.1021/jz4020162.
- [91] K. Manseki, T. Ikeya, A. Tamura, T. Ban, T. Sugiura, and T. Yoshida, "Mg-doped TiO₂ nanorods improving open-circuit voltages of ammonium lead halide perovskite solar cells," *RSC Adv.*, vol. 4, no. 19, pp. 9652–9655, 2014, doi: 10.1039/c3ra47870j.
- [92] H. S. Kim *et al.*, "Lead iodide perovskite sensitized all-solid-state submicron thin film mesoscopic solar cell with efficiency exceeding 9%," *Sci. Rep.*, vol. 2, pp. 1–7, 2012, doi: 10.1038/srep00591.
- [93] S. D. Stranks and H. J. Snaith, "Metal-halide perovskites for photovoltaic and light-emitting devices," *Nat. Nanotechnol.*, vol. 10, no. 5, pp. 391–402, 2015, doi: 10.1038/nnano.2015.90.
- [94] M. M. Lee, J. Teuscher, T. Miyasaka, T. N. Murakami, and H. J. Snaith, "Efficient hybrid solar cells based on Meso-structured organometal halide perovskites," vol. 338, no. November, pp. 643–648, 2012.
- [95] M. Petrović, V. Chellappan, and S. Ramakrishna, "Perovskites: Solar cells & engineering applications - materials and device developments," *Sol. Energy*, vol. 122, pp. 678–699, 2015, doi: 10.1016/j.solener.2015.09.041.
- [96] A. Rajagopal, K. Yao, and A. K. Y. Jen, "Toward Perovskite Solar Cell Commercialization: A Perspective and Research Roadmap Based on Interfacial Engineering," *Adv. Mater.*, vol. 30, no. 32, pp. 1–45, 2018, doi: 10.1002/adma.201800455.
- [97] J. M. Azpiroz, E. Mosconi, J. Bisquert, and F. De Angelis, "Defect migration in methylammonium lead iodide and its role in perovskite solar cell operation," *R. Soc. Chem.*, vol. 8, no. 7, pp. 2118–2127, 2015, doi: 10.1039/c5ee01265a.
- [98] Y. Liu *et al.*, "Stimulated emission from CsPbBr₃ quantum dot nanoglass," *Opt. Mater. Express*, vol. 9, no. 8, p. 3390, 2019, doi: 10.1364/ome.9.003390.
- [99] T. Xu, L. Chen, Z. Guo, and T. Ma, "Strategic improvement of the long-term stability of perovskite materials and perovskite solar cells," *Phys. Chem. Chem. Phys.*, vol. 18, no. 39, pp. 27026–27050, 2016, doi: 10.1039/c6cp04553g.
- [100] P. An, S. Thomson, M. Tesa, and A. Gakamsky, "Temperature-Dependent Absolute Photoluminescence Quantum Yield Measurements of a Halide P," *EDINBURGH INSTRUMENTS*, no. June, pp. 2–5, 2018.
- [101] Y. Wei *et al.*, "A CTAB-mediated antisolvent vapor route to shale-like Cs₄PbBr₆ microplates showing an eminent photoluminescence," *RSC Adv.*, vol. 10, no. 17, pp. 10023–10029, 2020, doi: 10.1039/c9ra10987k.
- [102] F. Di Stasio, S. Christodoulou, N. Huo, and G. Konstantatos, "Near-Unity Photoluminescence Quantum Yield in CsPbBr₃ Nanocrystal Solid-State Films via Postsynthesis Treatment with Lead Bromide," *Chem. Mater.*, vol. 29, no. 18, pp. 7663–7667, 2017, doi: 10.1021/acs.chemmater.7b02834.
- [103] S. Chatterjee, M. Ghosal, K. Tiwari, and P. Sen, "Potassium-Induced Passivation of Deep Traps in Bismuth-Doped Hybrid Lead Bromide Perovskite Nanocrystals: Massive Amplification of Photoluminescence Quantum Yield," *J. Phys. Chem. Lett.*, vol. 12, no. 1, pp. 546–551, 2021, doi: 10.1021/acs.jpcclett.0c03092.
- [104] Y. Khan *et al.*, "Waterproof perovskites: High fluorescence quantum yield and stability from a methylammonium lead bromide/formate mixture in water," *J. Mater. Chem. C*, vol. 8, no. 17, pp. 5873–5881, 2020, doi: 10.1039/d0tc00383b.

- [105] S. Lee *et al.*, “Versatile Defect Passivation Methods for Metal Halide Perovskite Materials and their Application to Light-Emitting Devices,” *Adv. Mater.*, vol. 31, no. 20, pp. 1–17, 2019, doi: 10.1002/adma.201805244.
- [106] J. C. Phys and O. F. Mohammed, “Near-unity photoluminescence quantum yield in inorganic perovskite nanocrystals by metal-ion doping Near-unity photoluminescence quantum yield in inorganic perovskite nanocrystals by metal-ion doping,” *Chem. Phys.*, vol. 020902, no. October 2019, p. 10, 2020, doi: 10.1063/1.5131807.
- [107] F. Liu *et al.*, “Highly Luminescent Phase-Stable CsPbI₃ Perovskite Quantum Dots Achieving Near 100% Absolute Photoluminescence Quantum Yield,” *ACS Nano*, vol. 11, no. 10, pp. 10373–10383, 2017, doi: 10.1021/acsnano.7b05442.
- [108] S. Wang *et al.*, *Cesium Lead Chloride/Bromide Perovskite Quantum Dots with Strong Blue Emission Realized via a Nitrate-Induced Selective Surface Defect Elimination Process*, vol. 10, no. 1. 2019.
- [109] M. Lu *et al.*, “Spontaneous Silver Doping and Surface Passivation of CsPbI₃ Perovskite Active Layer Enable Light-Emitting Devices with an External Quantum Efficiency of 11.2%,” *ACS Energy Lett.*, vol. 3, no. 7, pp. 1571–1577, 2018, doi: 10.1021/acsenerylett.8b00835.
- [110] S. F. Solari, S. Kumar, J. Jagielski, N. M. Kubo, F. Krumeich, and C. J. Shih, “Ligand-Assisted solid phase synthesis of mixed-halide perovskite nanocrystals for color-pure and efficient electroluminescence,” *J. Mater. Chem. C*, vol. 9, no. 17, pp. 5771–5778, 2021, doi: 10.1039/d0tc04667a.
- [111] K. Srisawad, P. Kanjanaboos, P. Wilairat, S. Sahasithiwat, and P. Pakawatpanurut, “Enhanced electroluminescence of cesium lead bromide light-emitting diode driven by ion migration via surface passivation with organic halide surfactants,” *Surfaces and Interfaces*, vol. 30, no. March, p. 101853, 2022, doi: 10.1016/j.surfin.2022.101853.
- [112] J. Park *et al.*, “A relationship between the surface composition and spectroscopic properties of cesium lead bromide (CsPbBr₃) perovskite nanocrystals: Focusing on photoluminescence efficiency,” *Nanoscale*, vol. 12, no. 3, pp. 1563–1570, 2020, doi: 10.1039/c9nr08516e.
- [113] Q. Wang, X. Zheng, Y. Deng, J. Zhao, Z. Chen, and J. Huang, “Stabilizing the α -Phase of CsPbI₃ Perovskite by Sulfobetaine Zwitterions in One-Step Spin-Coating Films,” *Joule*, vol. 1, no. 2, pp. 371–382, 2017, doi: 10.1016/j.joule.2017.07.017.
- [114] A. Marronnier *et al.*, “Anharmonicity and Disorder in the Black Phases of CsPbI₃ used for Stable Inorganic Perovskite Solar Cells,” *Am. Chem. Soc.*, vol. 3, pp. 1715–1717, 2018.
- [115] Y. Zhou and Z. Yixin, “Chemical stability and instability of inorganic halide perovskites,” *Energy Environ. Sci.*, no. 1, 2019, doi: 10.1039/c8ee03559h.
- [116] L. Protesescu *et al.*, “Nanocrystals of Cesium Lead Halide Perovskites (CsPbX₃, X = Cl, Br, and I): Novel Optoelectronic Materials Showing Bright Emission with Wide Color Gamut,” *Nano Lett.*, pp. 1–5, 2015, doi: 10.1021/nl5048779.
- [117] S. Dastidar *et al.*, “High Chloride Doping Levels Stabilize the Perovskite Phase of Cesium Lead Iodide,” *Nano Lett.*, vol. 16, no. 6, pp. 3563–3570, 2016, doi: 10.1021/acs.nanolett.6b00635.
- [118] K. S. Rao, K. El-Hami, T. Kodaki, K. Matsushige, and K. Makino, “A novel method for synthesis of silica nanoparticles,” *J. Colloid Interface Sci.*, vol. 289,

- no. 1, pp. 125–131, 2005, doi: 10.1016/j.jcis.2005.02.019.
- [119] J. P. Murphy, “NOVEL HYBRID PEROVSKITE COMPOSITES AND MICROSTRUCTURES : SYNTHESIS AND CHARACTERIZATION,” *Mont. Tech Libr.*, no. June, pp. 1–110, 2018.
- [120] Y. Hu *et al.*, “Bismuth Incorporation Stabilized α -CsPbI₃ for Fully Inorganic Perovskite Solar Cells,” *Am. Chem. Soc.*, vol. 2, no. 10, pp. 2219–2227, 2017, doi: 10.1021/acseenergylett.7b00508.
- [121] L. Protesescu *et al.*, “Nanocrystals of Cesium Lead Halide Perovskites (CsPbX₃, X = Cl, Br, and I): Novel Optoelectronic Materials Showing Bright Emission with Wide Color Gamut,” *Nano Lett.*, vol. 15, no. 6, pp. 3692–3696, 2015, doi: 10.1021/nl5048779.
- [122] X. Wu *et al.*, “Trap states in lead iodide perovskites,” *J. Am. Chem. Soc.*, vol. 137, no. 5, pp. 2089–2096, 2015, doi: 10.1021/ja512833n.
- [123] V. O. Eze, B. Lei, and T. Mori, “Air-assisted flow and two-step spin-coating for highly efficient CH₃NH₃PbI₃ perovskite solar cells,” *Jpn. J. Appl. Phys.*, vol. 55, no. 2, pp. 2–8, 2016.
- [124] M. Kumar *et al.*, “Thermo-optical correlation for room temperature synthesis: cold-sintered lead halides,” *J. Mater. Sci. Mater. Electron.*, vol. 30, no. 6, pp. 6071–6081, 2019, doi: 10.1007/s10854-019-00908-x.
- [125] E. Aleksanyan, A. Aprahamian, A. S. Mukasyan, V. Harutyunyan, and K. V. Manukyan, “Mechanisms of mechanochemical synthesis of cesium lead halides: pathways toward stabilization of α -CsPbI₃,” *J. Mater. Sci.*, vol. 55, no. 20, pp. 8665–8678, 2020, doi: 10.1007/s10853-020-04617-3.
- [126] T. Miyasaka, A. Kulkarni, G. M. Kim, S. Öz, and A. K. Jena, “Perovskite Solar Cells: Can We Go Organic-Free, Lead-Free, and Dopant-Free?,” *Adv. Energy Mater.*, vol. 10, no. 13, 2020, doi: 10.1002/aenm.201902500.
- [127] N.-K. Cho, H.-J. Na, J. Yoo, and Y. S. Kim, “Long-term stability in γ -CsPbI₃ perovskite via an ultraviolet-curable polymer network,” *Commun. Mater.*, vol. 2, no. 1, pp. 1–8, 2021, doi: 10.1038/s43246-021-00134-1.
- [128] Y. Ji *et al.*, “Improving the Stability of α -CsPbI₃ Nanocrystals in Extreme Conditions Facilitated by Mn²⁺ Doping,” *ACS Omega*, vol. 6, no. 21, pp. 13831–13838, 2021, doi: 10.1021/acsomega.1c01383.
- [129] C. Bi, S. V. Kershaw, A. L. Rogach, and J. Tian, “Improved Stability and Photodetector Performance of CsPbI₃ Perovskite Quantum Dots by Ligand Exchange with Aminoethanethiol,” *Adv. Funct. Mater.*, vol. 29, no. 29, pp. 1–9, 2019, doi: 10.1002/adfm.201902446.
- [130] L. Zhang *et al.*, “All-Inorganic CsPbI₃ Quantum Dot Solar Cells with Efficiency over 16% by Defect Control,” *Adv. Funct. Mater.*, vol. 31, no. 4, pp. 1–10, 2021, doi: 10.1002/adfm.202005930.
- [131] Y. Shao *et al.*, “Designable and highly stable emissive CsPbI₃ perovskite quantum dots/polyvinylidene fluoride nanofiber composites,” *Opt. Mater. Express*, vol. 12, no. 1, p. 109, 2022, doi: 10.1364/ome.448282.
- [132] L. C. Chen *et al.*, “Red Light-Emitting Diodes with All-Inorganic CsPbI₃/TOPO Composite Nanowires Color Conversion Films,” *Nanoscale Res. Lett.*, vol. 15, no. 1, 2020, doi: 10.1186/s11671-020-03430-w.